Electrochimica Acta 323 (2019) 134791

Contents lists available at ScienceDirect

Electrochimica Acta

journal homepage: www.elsevier.com/locate/electacta

# Mechanism and effect of thermal degradation on electrolyte ionic diffusivity in Li-ion batteries: A molecular dynamics study

Tianhan Gao [a], Wei Lu [a, b, *]

[a] Department of Mechanical Engineering, University of Michigan, Ann Arbor, MI, 48109, USA
[b] Department of Materials Science and Engineering, University of Michigan, Ann Arbor, MI, 48109, USA

ARTICLE INFO

*Article history:*
Received 31 May 2019
Received in revised form
2 August 2019
Accepted 29 August 2019
Available online 4 September 2019

*Keywords:*
Lithium-ion battery
Electrolyte thermal degradation
Diffusivity
Solvent structure
MD simulation

ABSTRACT

Electrolyte ionic diffusivity significantly affects the power density and useable energy density of a lithium ion battery. During usage, electrolyte can decompose, leading to reduced ionic diffusivity. Understanding the degradation mechanism and its effect on ionic diffusivity is important for both battery design optimization to provide superior performance with a long cycle life and for better battery management during usage to extend the battery life. In this research, the ionic diffusivity of key electrolytes and their degradation, including DMC-$LiPF_6$, EMC-$LiPF_6$ and DEC-$LiPF_6$, are quantitatively predicted with classical and ReaxFF molecular dynamics simulations. The electrolyte solvent structures and reaction pathways are characterized. The effect of temperature, salt concentration and degree of thermal degradation on electrolyte ionic diffusivity are identified. A list of gas-phase, solvent-phase and solid-phase degradation products are categorized. DMC-$LiPF_6$ shows the highest thermal stability, while DEC-$LiPF_6$ shows the lowest thermal stability because of a large amount of $-CH_3CH_2$ group in the molecule. $PF_6^-$ tends to decompose first. The decomposed product of $PF_5$ can further lead to C—O bond breaking in solvent molecules, causing them to decompose into products composed of smaller molecules. Simulations show that the diffusion coefficients of cations and anions decrease with thermal degradation. The mechanism is found to be related to the clustering of $Li^+$, R-$O^-$ and $(R-OCO_2)^-$, which impedes ion diffusion in the electrolyte. This paper provides a quantitative understanding of electrolyte thermal degradation, revealing the underlying mechanisms and effects on electrolyte properties at the atomistic level by a systematic comparative study for the first time. The approach will provide valuable guidance to the development of lithium ion batteries.



## 1. Introduction

Lithium ion battery (LIB) is widely used in a wide range of fields, from smart phones, laptops, electric vehicles to satellites [1,2]. Various attempts have been made to increase the rate performance and energy density, which will generate more heat inside a battery. Even with external cooling, the battery will operate at higher internal temperatures. Overcharging or thermal runaway can further increase the local temperature. In addition, some types of LIBs need to work in extreme heat environments. Combining with the difficulty of thermal management, the temperature inside a LIB can increase easily during usage. The electrolytes in current LIBs are mostly organic solvents dissolved with lithium hexafluorophosphate ($LiPF_6$) salt. The widely used organic solvents include Dimethyl Carbonate (DMC), Ethyl Methyl Carbonate (EMC), Diethyl Carbonate (DEC), Ethylene Carbonate (EC), Propylene Carbonate (PC), which have relatively high electrochemical stability but poor thermal stability, especially with $LiPF_6$ salt [3]. They can easily undergo thermal degradation at an elevated temperature (above 60°C–70 °C) [4–8]. Some thermal degradation products of the $LiPF_6$ salt can act as catalyst to accelerate the degradation of organic solvent, forming chain reactions and causing more electrolyte degradation [9,10]. Thermal degradation has a significant negative impact on the properties of electrolyte, especially on ionic diffusivity. Understanding the thermal degradation mechanism and its effect can help design better LIBs, develop strategies to maintain the battery performance, and provide guidance for advanced battery management system.

Thermal degradation of electrolyte has started to emerge as an

* Corresponding author. Department of Mechanical Engineering, University of Michigan, Ann Arbor, MI, 48109, USA.
*E-mail address:* weilu@umich.edu (W. Lu).

https://doi.org/10.1016/j.electacta.2019.134791
0013-4686/

important research topic. Lamb et al. [11] used experimental methods to investigate the thermal degradation products of electrolytes, especially gas-phase products. The electrolyte solutions investigated included DMC, EMC, DEC and EC solvent with $LiPF_6$ salt. It was found that EC and DEC mainly contribute to the gas product during thermal degradation while DMC is relatively stable, and $LiPF_6$ can affect the thermal degradation rate of EMC. They also found that the gas products are highly combustible. Ravdel et al. [3] experimentally investigated the thermal decomposition of $LiPF_6$ in solid and solution states (with dialkyl carbonate solvent). Conductivity is directly related to diffusivity and is easier to measure. The conductivity of thermally degraded electrolytes including DMC-$LiPF_6$ and EC/DMC/DEC-$LiPF_6$ was measured. It was shown that the thermal degradation of dialkyl carbonate-$LiPF_6$ electrolyte can generate $PF_5$, $CO_2$, ethers and alkyl fluorides, among other products. The conductivity of EC/DMC/DEC-$LiPF_6$ electrolyte was found to decrease linearly during the heating period, while the conductivity of DMC-$LiPF_6$ electrolyte decreased at an increasing rate during heating. Despite these studies, the detailed thermal degradation process and mechanism, as well as the mechanism of thermally degraded electrolyte on ionic diffusivity, remained unclear. It is difficult to experimentally capture the complex thermal degradation process and the intrinsic mechanism. Molecular simulations can provide important insights.

Molecular dynamics (MD) simulations have been used recently to reveal the characteristics of electrolytes. Ravikumar et al. [12] investigated the effect of $LiPF_6$ salt concentration on ionic diffusivity and the corresponding conductivity by Einstein's relation, showing a maximum conductivity at the salt concentration of 1 M. Kumar et al. [13] investigated the behavior of $LiPF_6$ in EC solvent, using both MD and *ab initio* density functional theory (DFT) calculations. Their work focused on the solvent structure with $Li^+$ and $PF_6^-$ ions, and showed that the intermolecular and intramolecular potentials can produce essential features of the electrolyte. Their work highlighted that using MD simulations with proper force fields, ion dynamics and thermodynamics in the electrolyte can be well captured. Ong et al. [14] investigated the solvation and diffusion of $Li^+$ ion in EC, EMC and EC/EMC with *ab initio* MD simulations, showing that $Li^+$ ion can be solvated by carbonyl, oxygen atoms of the solvent, or $PF_6^-$ ions. The diffusion coefficient of $Li^+$ ion in EMC was shown to be larger than that in EC, and the diffusion coefficient of $PF_6^-$ ion was higher than that of $Li^+$ ion. These works on regular, non-degraded electrolytes suggested MD simulation as a powerful tool to investigate ion diffusion in different types of electrolytes with different solvent structures.

For the study of thermal degradation of electrolytes, reactive force field (ReaxFF) MD simulations are highly useful [15]. ReaxFF is able to describe bond breaking, bond formation and chemical reactivity, and the force field parameters are obtained from an extensive training set of geometrical and energetic data from quantum mechanics calculations [16]. Cao et al. [17] used ReaxFF MD simulations to investigate the thermal decomposition of HFO-1234yf with $O_2$ in a wide range of temperatures. Chenoweth et al. [18] investigated the thermal decomposition of poly(-dimethylsiloxane) polymer, and demonstrated ReaxFF as a powerful computational tool for studying the chemical stability of polymers. Diao et al. [19] investigated the thermal decomposition of epoxy resin, and concluded that ReaxFF can provide useful insights into the complicated bulk thermal decomposition of organic materials under extreme conditions at the atomistic level. However, there are few researches focusing on the thermal degradation simulation of LIB electrolytes.

In this research, the mechanism of electrolyte degradation and its effect were investigated using molecular dynamics simulations. The ionic diffusivity of three types of electrolytes, including DMC-$LiPF_6$, EMC-$LiPF_6$ and DEC-$LiPF_6$ without degradation, was calculated and analyzed first with classical MD simulations. Then ReaxFF MD simulations were performed to simulate and analyze the degradation process of each electrolyte under different salt concentrations. The degradation products were categorized. Finally, the ionic diffusivity of each electrolyte with different degree of degradation was calculated for different temperatures and initial salt concentrations. The effect of degraded electrolyte products on ionic diffusivity was studied based on solvent structural analysis. These studies provided a quantitative understanding of thermal degradation in electrolytes, and revealed the underlying mechanisms and effects on electrolyte structures and ionic diffusivity at the atomistic level.

## 2. Simulation set-up and methods

### 2.1. Classical MD simulation for undegraded electrolyte

The ionic diffusion coefficient can be calculated by the following equation:

$$D_i = \lim_{t\to\infty} \frac{MSD^i}{6t} \left( \mathrm{i} = \mathrm{cation},\ \mathrm{anion} \right) \quad (1)$$

where $t$ denotes time (s), $D_{cation}$ and $D_{anion}$ denote the diffusion coefficient of cations and anions in the electrolyte ($m^2/s$), which are calculated by the mean square displacement (MSD) of cations and anions. In the classical MD simulation, the Class II force field was used to calculate the interaction among atoms and ions. Specifically, the CFF91 force field was chosen in this research. For the 12-6 LJ pair interaction, a cutoff distance of 12 Å was used. The particle−particle−particle−mesh (PPPM) method was employed to compute the long-range Coulombic interaction.

The electrolyte diffusivity without thermal degradation was investigated first, in order to provide a basic understanding of ion dynamics inside undecomposed electrolytes. Three types of electrolytes, DMC-$LiPF_6$, EMC-$LiPF_6$ and DEC-$LiPF_6$, were considered. The solvent molecules all have linear structures, as shown in Fig. 1(a). The Forcite module in Materials Studio software was employed to conduct classical MD simulations. The COMPASS force field was used to calculate the LJ parameters and partial charges. The partial charges of atoms in solvent and salt molecules are shown in Fig. 1(a). The PCFF force field and parameters (based on the CFF91 force field) were employed in the MD simulation.

For the simulation model, 150 solvent molecules (either DMC, EMC or DEC) were put inside a simulation box with periodic boundaries. The number of $LiPF_6$ salt molecule was set to be 15 or 21 in different models to make the molar ratio of salt molecule to solvent molecule (denoted by $r(LiPF_6)$) to be 0.10 or 0.14, respectively. Molecules and ions were placed at random positions initially. In this paper $r(LiPF_6)$ is used to represent the initial electrolyte salt concentration. The simulation models for DMC-$LiPF_6$, EMC-$LiPF_6$ and DEC-$LiPF_6$ electrolytes with $r(LiPF_6)$ 0.10 are shown in Fig. 1(b). The detailed simulation set-up information is given in Table 1. The initial density of each simulation was set to be 1.1 $g/cm^3$. Three temperatures, 333 K, 303 K and 283 K, were selected in this research to cover the typical temperature range of actual LIB usage. In MD simulations, the time step was set to be 1.0 fs, the NPT ensemble was firstly employed to conduct the simulation for 500 ps to relax the system from its initial configuration. The pressure for the NPT relaxation was set to be 1 atm. The resulting density after

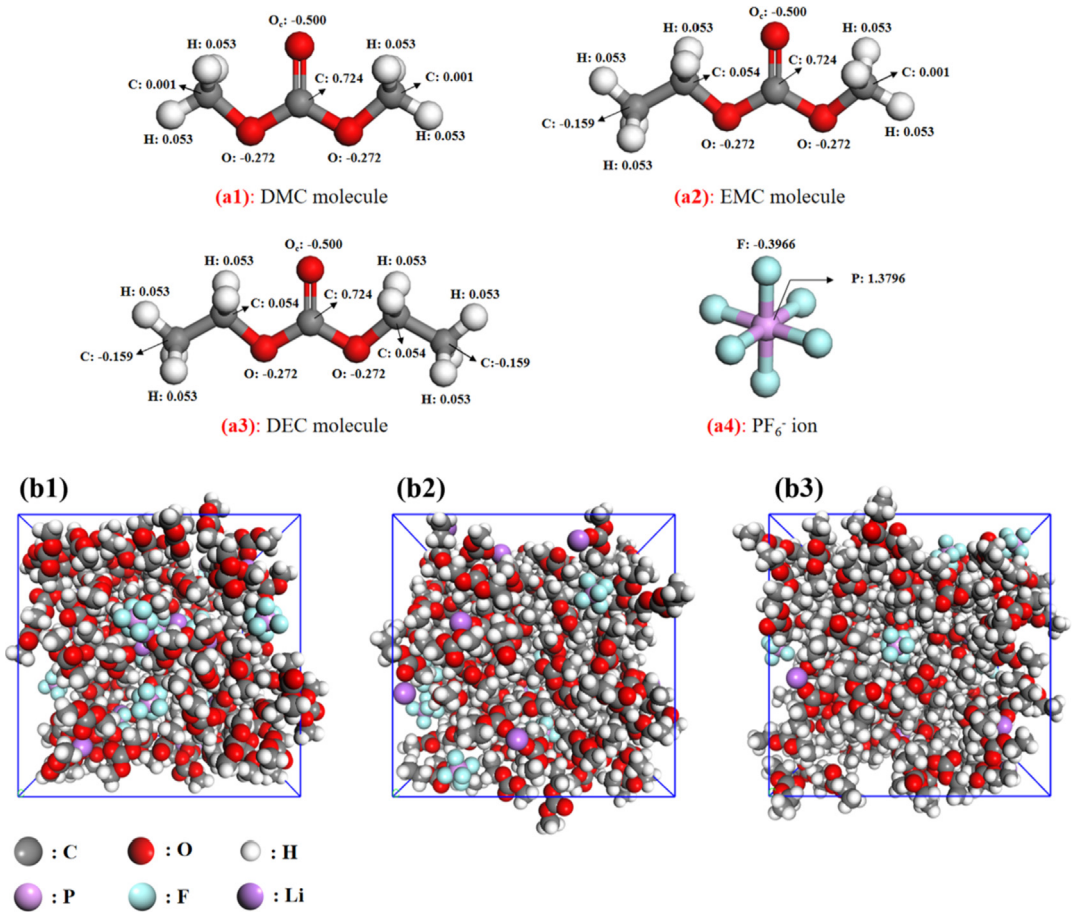


**Fig. 1.** (a) Structures of electrolyte molecule and calculated charge of each atom in the molecule. (b) Configuration of the simulation system for each type of electrolyte with an initial salt concentration of $r(LiPF_6) = 0.1$. (b1) DMC-$LiPF_6$ electrolyte, (b2) EMC-$LiPF_6$ electrolyte, (b3) DEC-$LiPF_6$ electrolyte.

**Table 1**
Detailed set-up information for ionic diffusivity simulation in electrolyte without thermal degradation.

| Simulation group No. | Electrolyte type | Number of solvent molecules | Number of salt molecules | Molar ratio ($r(LiPF_6)$) | Simulation temperature (K) | Density after NPT relaxation (g/cm$^3$) |
|---|---|---|---|---|---|---|
| 1 | DMC-$LiPF_6$ | 150 | 15 | 0.10 | 333 | 1.185 |
| 2 | | | | | 303 | 1.217 |
| 3 | | | | | 283 | 1.233 |
| 4 | | | 21 | 0.14 | 333 | 1.224 |
| 5 | | | | | 303 | 1.257 |
| 6 | | | | | 283 | 1.278 |
| 7 | EMC-$LiPF_6$ | 150 | 15 | 0.10 | 333 | 1.106 |
| 8 | | | | | 303 | 1.133 |
| 9 | | | | | 283 | 1.150 |
| 10 | | | 21 | 0.14 | 333 | 1.123 |
| 11 | | | | | 303 | 1.256 |
| 12 | | | | | 283 | 1.277 |
| 13 | DEC-$LiPF_6$ | 150 | 15 | 0.10 | 333 | 1.034 |
| 14 | | | | | 303 | 1.063 |
| 15 | | | | | 283 | 1.079 |
| 16 | | | 21 | 0.14 | 333 | 1.065 |
| 17 | | | | | 303 | 1.095 |
| 18 | | | | | 283 | 1.113 |

NPT relaxation is presented in Table 1. Then, the NPT ensemble was removed, and the NVT ensemble was used to conduct the simulation for 1000 ps. The characteristics of ion motion was distilled from the NVT simulation to investigate the ion dynamics in the electrolyte under different temperatures and salt concentrations. We tested simulations starting with different initial positions of molecules and ions. We found that the 500 ps relaxation step was sufficient for the system to reach its preferred configuration, making the system characteristics such as calculated diffusion coefficient independent of the initial positions of molecules and ions.

### 2.2. ReaxFF MD simulation for electrolyte thermal degradation process

With ReaxFF, the energy function is given in the following form [15].

$$E_{system} = E_{bond} + E_{over} + E_{under} + E_{val} + E_{pen} + E_{conj} + E_{tors} + E_{vdW} + E_{coulomb} \quad (2)$$

where $E_{system}$ represents the total energy of the simulation system, $E_{bond}$ represents the bond energy, $E_{over}$ and $E_{under}$ denote the over-coordinated and under-coordinated energy respectively, $E_{val}$, $E_{pen}$, $E_{conj}$, $E_{tors}$, $E_{vdW}$ and $E_{Coulomb}$ represent the valence angle term, penalty energy, conjugation effects to molecular energy, torsion energy, non-bonded van der Waals interaction and Coulomb interaction, respectively [15].

The ReaxFF module in LAMMPS (Large Scale Atomic/Molecular Massively Parallel Simulator) software was employed in this research to simulate the thermal degradation of electrolytes. The ReaxFF force field parameters for C/H/O/F/P/Li were obtained from the references of van Duin et al. [15], Han et al. [20], Islam et al. [21], Bedrov et al. [22] and Abolfath et al. [23]. For the simulation model, 150 solvent molecules (either DMC, EMC or DEC) were put inside a simulation box with periodic boundaries. The number of $LiPF_6$ salt molecule was set to be 15 or 21 in different models to make the molar ratio of salt molecule to solvent molecule to be 0.10 or 0.14, respectively. The density of the simulation system was selected to be the value after NPT relaxation (at 333 K) in Table 1. The detailed set-up information for the ReaxFF simulation is given in Table 2. The simulation time was set to be 20 ps with a time step of 0.1 fs. Significant thermal degradation of LIB electrolyte at room temperature (20°C–35 °C) or at modest elevated temperature (60°C–85 °C) can take a long time to occur, from 24 h to several months [3,5]. The practical ReaxFF MD simulation time is much shorter. Therefore, we applied a strategy of accelerated simulation by increasing the temperature, which has been widely used by many scholars when conducting ReaxFF MD simulations [16,17,19,24,25]. Our ReaxFF MD simulations were performed at 400 K, 600 K, 800 K and 1000 K for the DMC-$LiPF_6$ electrolyte, at 400 K, 600 K, 700 K and 800 K for the EMC-$LiPF_6$ electrolyte, and at 400 K, 600 K and 700 K for the DEC-$LiPF_6$ electrolyte. We performed all simulations for the same duration of 20 ps, therefore, the results at a higher simulation temperature correspond to a longer actual time. The exact mapping of temperature to actual time needs experiments, but in this research we focus on the ranking of electrolyte degradation so that time mapping is not necessary.

### 2.3. MD simulation for the degraded electrolyte ionic diffusivity

After ReaxFF MD simulations of electrolyte degradation, classical MD simulations were again performed to investigate the ionic diffusivity of electrolytes after different degrees of thermal degradation. Materials Studio was again employed to conduct the classical MD simulations. The COMPASS and PCFF force field were implemented to account for interaction between atoms and ions. The COMPASS force field was mainly used to calculate the LJ parameters and partial charges, while the PCFF force field was used to conduct the classical MD simulation for the ion diffusion.

Same as section 2.1, a cutoff distance of 12 Å was used for the 12-6 LJ pair interaction and the PPPM method was employed to compute the long-range Coulombic interaction.

The ReaxFF MD simulations generated various products in the solvent phase as well as in the gas and solid phase. We transferred all the molecules and their corresponding amount in the solvent phase to the classical MD simulations to investigate the resulting ionic diffusivity of electrolytes after thermal degradation. Each system was firstly relaxed with NPT for 500 ps. The pressure was set to be constant as 1 atm, while the temperature was set to be 283 K, 303 K and 333 K, respectively. Then each simulation was conducted with NVT for 1000 ps at the same constant temperature as the preceding NPT relaxation simulation. The MSD of cations and anions was distilled from the NVT simulation. The time step for the classical MD simulation was 1 fs.

## 3. Results and discussions

### 3.1. Results of the ionic diffusivity in undegraded electrolyte

We first performed classical MD simulations to investigate the ionic diffusivity of undegraded electrolyte using the method in section 2.1. The average MSD of cations ($Li^+$) and anions ($PF_6^-$) in each electrolyte was distilled. The result for a salt concentration of $r(LiPF_6) = 0.10$ at temperature 333 K is shown in Fig. 2(a). It can be seen that the MSD of $Li^+$ and $PF_6^-$ increases almost linearly with time, suggesting that the diffusion of these ions is relatively uniform. The average MSD curve of each type of electrolyte at different temperatures was distilled. Each curve was fitted by a straight line using linear regression. The slope of the line was used to calculate the diffusion coefficient by Eq. (1). The results are shown in Fig. 2(b). It can be seen that the diffusion coefficient increases with temperature. At the same temperature, the ions in the EMC-$LiPF_6$ electrolyte have the highest diffusion coefficient, followed by the DEC-$LiPF_6$ electrolyte. The ions in the DMC-$LiPF_6$ electrolyte have the lowest diffusion coefficient. These suggest that EMC has the highest ability to diffuse $Li^+$ and $PF_6^-$, while DMC has the least ability. By calculating the ratio of diffusion coefficient between $PF_6^-$ and $Li^+$ ions at the three simulation temperatures and then taking average of the three ratios, we find that by average the diffusion coefficient of $PF_6^-$ is about 22.34%, 8.01% and 9.82% higher than that of $Li^+$ in the DMC-$LiPF_6$, EMC-$LiPF_6$, and DEC-$LiPF_6$ electrolytes, respectively. This suggest that $PF_6^-$ diffuses faster than $Li^+$ in the three types of electrolytes in the temperature window studied, although $PF_6^-$ ions are larger and heavier than $Li^+$ ions. The largest relative difference occurs in the DMC-$LiPF_6$ electrolyte. To understand why $Li^+$ diffuses slower than $PF_6^-$, we calculated the radial distribution function (defined in section 3.3), which quantified the pair correlation between the ions and solution molecules. We found that $Li^+$ ions are easily absorbed by solvent molecules and form bulk clusters, which causes them to diffuse slower than $PF_6^-$ ions.

**Table 2**
Detailed ReaxFF set-up information for simulation of electrolyte thermal degradation.

| Simulation group No. | Electrolyte type | Number of solvent molecules | Number of salt molecules | Molar ratio ($r(LiPF_6)$) | Density after NPT relaxation (g/cm$^3$) |
|---|---|---|---|---|---|
| 1 | DMC-$LiPF_6$ | 150 | 15 | 0.10 | 1.185 |
| 2 | | | 21 | 0.14 | 1.224 |
| 3 | EMC-$LiPF_6$ | 150 | 15 | 0.10 | 1.106 |
| 4 | | | 21 | 0.14 | 1.123 |
| 5 | DEC-$LiPF_6$ | 150 | 15 | 0.10 | 1.034 |
| 6 | | | 21 | 0.14 | 1.065 |

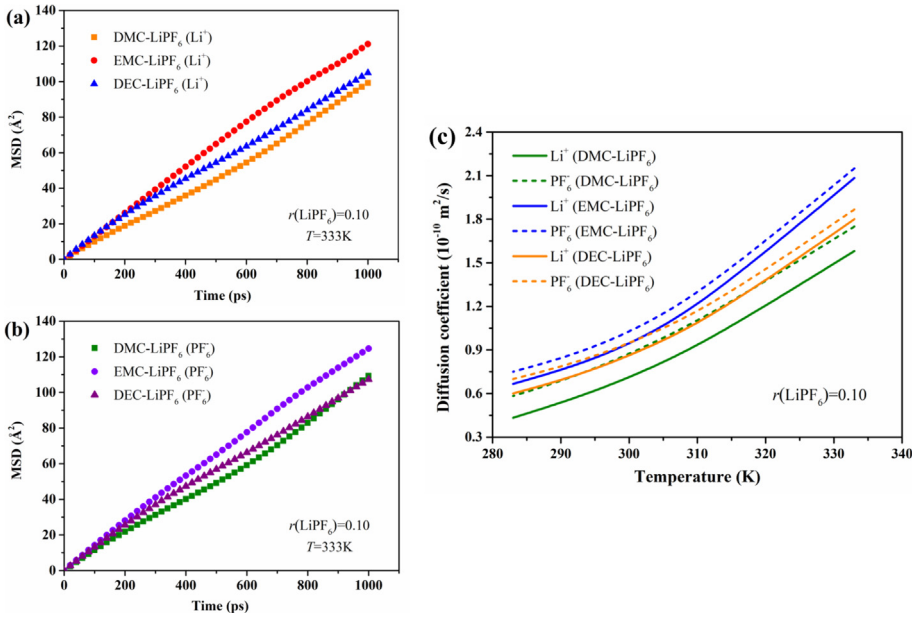


**Fig. 2.** (a) Average MSD curves of $Li^+$ and $PF_6^-$ ions in three types of electrolytes (Temperature: 333 K). (b) Diffusion coefficient of $Li^+$ and $PF_6^-$ ions in three types of electrolytes. The salt concentration is $r(LiPF_6) = 0.10$.

Fig. 3(a) shows the results for a salt concentration of $r(LiPF_6) = 0.14$. In comparison to the results in Fig. 2(a) at the same temperature, we can observe that the slopes of MSD curves are smaller, suggesting slower diffusion at this higher salt concentration. Fig. 3(b) shows that the diffusion coefficient increases with temperature, and $PF_6^-$ diffuses faster than $Li^+$. By average, the diffusion coefficient of $PF_6^-$ is about 19.07%, 5.60% and 12.86% larger than that of $Li^+$ in the DMC-$LiPF_6$, EMC-$LiPF_6$ and DEC-$LiPF_6$ electrolytes, respectively. Note that when the temperature is lower than 298 K, $Li^+$ ions in the DEC-$LiPF_6$ electrolyte has a lower diffusion coefficient than in the EMC-$LiPF_6$ electrolyte. However, when the temperature is higher than 298 K, the diffusion coefficient of $Li^+$ ions in the DEC-$LiPF_6$ electrolyte increases significantly with temperature, and surpasses the diffusion coefficient in the EMC-$LiPF_6$ electrolyte. This indicates that the diffusion of $Li^+$ in DEC-$LiPF_6$ is more sensitive to temperature than that in EMC-$LiPF_6$ at a salt concentration of $r(LiPF_6) = 0.14$.

It should be noted that we have performed benchmark simulations and compared them with experimental results and other MD simulations in the literature, to validate the accuracy of MD simulations in quantifying ion diffusion in electrolytes. The EC-$LiPF_6$ electrolyte was taken as a benchmark due to the availability of simulations and experiments for $Li^+$ and $PF_6^-$ diffusion in the EC solvent [12,13,26,27]. The set-up of the benchmark MD simulation is shown in Fig. 4(a), where 150 EC molecules and 15 $LiPF_6$ molecules were put inside the simulation box with periodic boundaries.

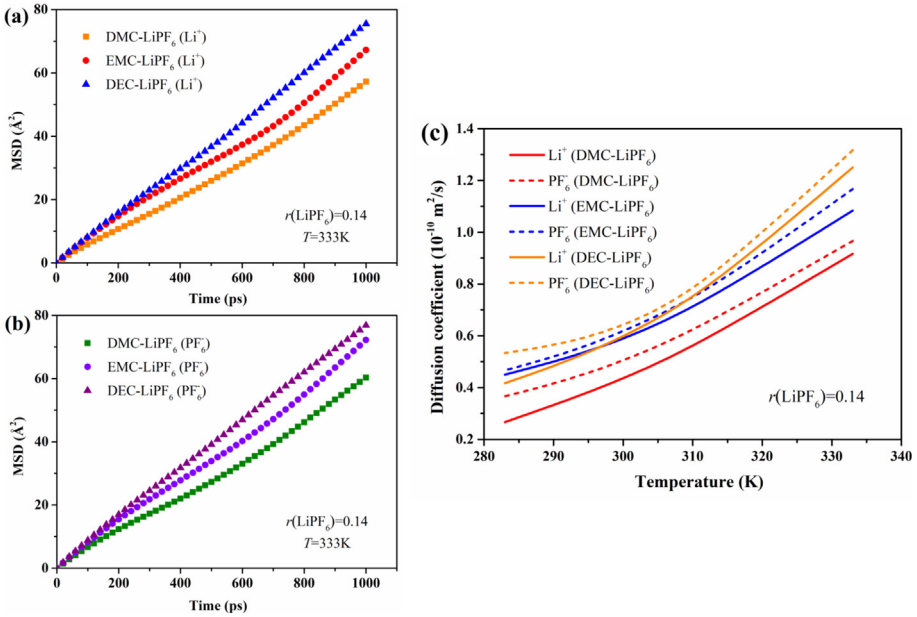


**Fig. 3.** (a) Average MSD curves of $Li^+$ and $PF_6^-$ ions in three types of electrolytes. (Temperature: 333 K). (b) Diffusion coefficient of $Li^+$ and $PF_6^-$ ions in three types of electrolytes. The salt concentration is $r(LiPF_6) = 0.14$.

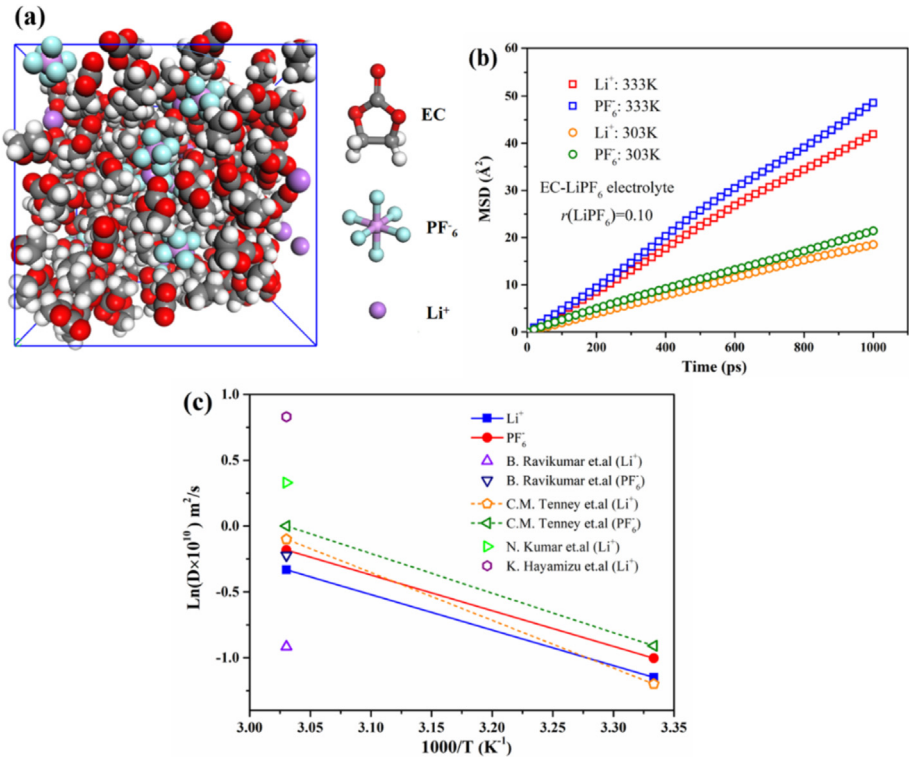


**Fig. 4.** Results for benchmark EC-$LiPF_6$ electrolyte at a salt concentration of $r(LiPF_6) = 0.10$. (a) A snapshot of the benchmark classical MD simulation set-up. (b) Average MSD of $Li^+$ and $PF_6^-$ ions in the EC-$LiPF_6$ electrolyte at 333 K and 303 K. (c) Comparison with results and data from the literature [12,13,26,27].

This gives a salt molar concentration of 1.04 M. The initial density of the simulation system was set to be 1.32 g/cm$^3$. The same procedure as in section 2.1 was used, i.e. first relaxing the system by NPT for 500 ps under 1 atm pressure, followed by NVT for 1000 ps with a time step of 1.0 fs. The simulations were performed for two temperatures of 333 K and 303 K. Fig. 4(b) shows the MSD curves. The slope for $PF_6^-$ is 24.8% and 17.6% larger than that for $Li^+$ at 333 K and 303 K, respectively. The diffusion coefficients were calculated based the MSD curves and compared with the values in the literature [12,13,26,27], as shown in Fig. 4(c). The obtained values are within those reported by other researchers. The comparison confirms that the classical MD simulation employed in this research is appropriate to quantify ion diffusion in electrolytes.

### 3.2. Results of thermal degradation simulation

In this section, the ReaxFF-MD simulation results for the thermal degradation of electrolytes are analyzed and discussed. We started with a salt concentration of $r(LiPF_6) = 0.10$. Fig. 5 shows the number of degraded solvent and salt molecules at different temperatures. The number of degraded solvent molecules is obtained by counting the number of solvent molecules that change to other type of products. The number of degraded salt molecules is obtained by counting the number of $PF_6^-$ ions in the $LiPF_6$ salt molecules that change to other type of products. It can be observed that the number of degraded solvent and salt molecules increases with the ReaxFF simulation temperature (RST). In the DMC-$LiPF_6$ electrolyte, the degradation of solvent molecule is slow at the beginning, with a rate of 0.0075/K, but increases rapidly when the RST is above 800 K, to a rate of 0.06/K. By contrast, the salt degradation rate is relatively uniform with increasing RST. For the EMC-$LiPF_6$ and DEC-$LiPF_6$ electrolytes, the solvent and salt degradation rate is higher than that of the DMC-$LiPF_6$ electrolyte. The degradation rate increases rapidly when the RST is higher than 600 K, reaching 0.08/

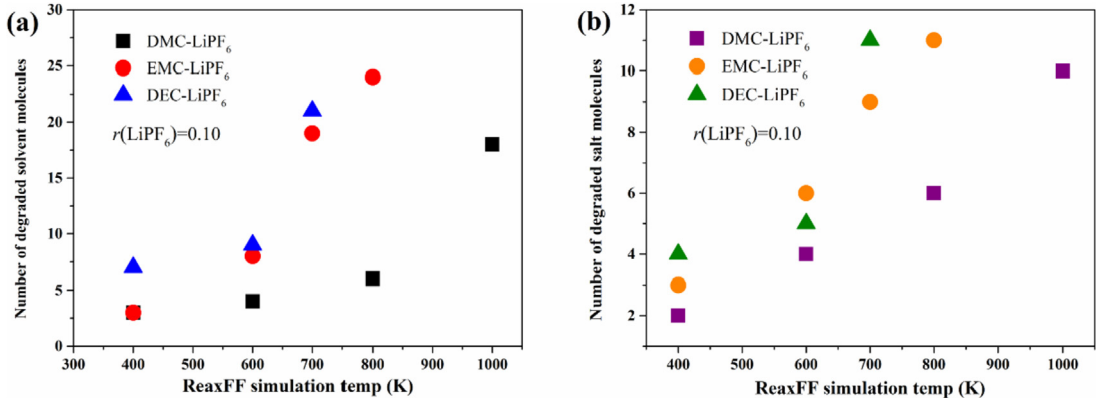


**Fig. 5.** Number of degraded molecules in three electrolytes under various ReaxFF simulation temperatures (RST). (a) Solvent molecule, (b) $LiPF_6$ salt molecule. Salt concentration at $r(LiPF_6) = 0.10$.

K and 0.12/K for EMC and DEC solvent molecules, respectively. The degradation rate is 0.025/K and 0.06/K for the $LiPF_6$ salt molecules in the EMC-$LiPF_6$ and DEC-$LiPF_6$ electrolytes, respectively. These results show that the DMC-$LiPF_6$ electrolyte has the highest stability against thermal degradation, with both solvent and salt having the lowest degradation rate. The EMC-$LiPF_6$ electrolyte has a lower stability, while the DEC-$LiPF_6$ electrolyte has the lowest stability. This trend is consistent with experimental observations [11].

Fig. 6 shows the type and amount of degraded products in each electrolyte. Fig. 6(a) shows the gas-phase products. Fig. 6(b) shows the solvent-phase products without fluorine element. Fig. 6(c) shows the solvent-phase products having fluorine element plus the solid-phase product of LiF.

As shown in Fig. 6(a1), the gas-phase degradation products in the DMC-$LiPF_6$ electrolyte are $CO_2$ and $CH_3F$, which increase with RST. Notably, when the temperature increases from 800 K to 1000 K, the number of $CO_2$ and $CH_3F$ molecules increases rapidly. For the solvent-phase products without fluorine element in Fig. 6(b1), both $(CH_3OCO_2)^-$ and $CH_3O^-$ anions appear when the RST is 600 K. The amount of $(CH_3OCO_2)^-$ anions increases slightly when the RST increases from 600 K to 800 K. However, when the RST is 1000 K, the $(CH_3OCO_2)^-$ anions become completely decomposed. By contrast, the amount of $CH_3O^-$ anions continues increasing with RST, with a large increase when the RST changes from 800 K to 1000 K. For the solvent-phase product having fluorine element in Fig. 6(c1), the $PF_5$ molecule, which is decomposed from $PF_6^-$, dominates the fluorine-containing degradation products. A small amount of $(CH_3OFCO_2CH_3)^-$ anions are initially generated but disappear due to thermal decomposition when the RST is higher than 800 K. The $CH_3OCFO$ molecule is generated when the RST is 1000 K. These results show that $(CH_3OCO_2)^-$ and $(CH_3OFCO_2CH_3)^-$ are not stable, which can be easily generated but become decomposed later along with the continuing thermal degradation process. $CH_3O^-$ anions and $PF_5$ molecules are relatively stable, which do not appear to react with other molecules or ions.

More types of gas-phase products are generated during the thermal degradation of EMC-$LiPF_6$ electrolyte, especially when the RST is higher than 400 K. Fig. 6(a2) shows that initially only $CH_3CH_2F$ molecules are generated. Further thermal degradation leads to the production of $CO_2$ and $CH_3F$ molecules. Then $H_2$, $C_2H_4$, $C_2H_6$ and $CH_2F_2$ molecules are generated when the RST is 800 K. The amount of $CO_2$ and $CH_3F$ molecules increases with RST, while the amount of $CH_3CH_2F$ molecules almost remains constant. Also, the amount of $CH_3CH_2F$ molecules is smaller than that of $CO_2$ and $CH_3F$ molecules.

As for the gas-phase products of DEC-$LiPF_6$ electrolyte, Fig. 6(a3) shows that $CH_3F$ molecules are not generated during the entire thermal degradation process. $CH_3CH_2F$ and $C_2H_4$ molecules are generated in a large amount, which increases significantly with RST. Besides, $CO_2$ molecules are generated, but the amount is relatively stable in comparison to $CH_3CH_2F$ and $C_2H_4$ products. When the RST is higher than 400 K, a small amount of $H_2$ molecules are also generated.

The solvent-phase products of EMC-$LiPF_6$ and DEC-$LiPF_6$ show more types than DMC-$LiPF_6$, as can be seen in Fig. 6(b2, b3) and (c2, c3). In the EMC-$LiPF_6$ electrolyte, the amount of generated $(CH_3OCO_2)^-$ ions initially decreases and then increases when the RST changes from 400 K to 800 K. This indicates that the generation and decomposition of $(CH_3OCO_2)^-$ anions can occur simultaneously during the thermal degradation process. The generation rate of $(CH_3OCO_2)^-$ anions finally surpasses the decomposition rate. The $(CH_3CH_2OCO_2)^-$ anions are initially generated and then completely decomposed when the RST increases from 600 K to 800 K, suggesting that $(CH_3CH_2OCO_2)^-$ anions have less thermal stability than $(CH_3OCO_2)^-$ anions. $CH_3O^-$ and $CH_3CH_2O^-$ anions are generated

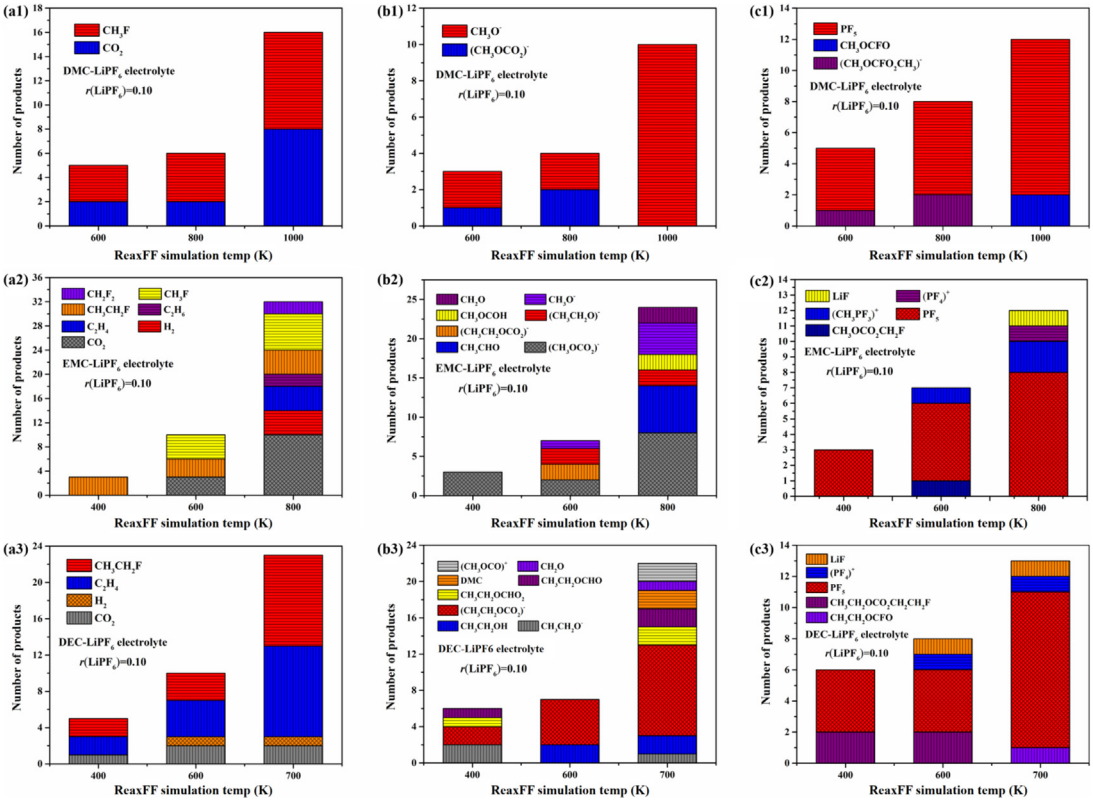


**Fig. 6.** Type and amount of degraded products from ReaxFF MD simulations at a salt concentration of $r(LiPF_6) = 0.10$. (a1-c1) DMC-$LiPF_6$ electrolyte, (a2-c2) EMC-$LiPF_6$ electrolyte, (a3-c3) DEC-$LiPF_6$ electrolyte.

when the RST is 600 K. The amount of $CH_3O^-$ ions increases significantly with RST, while the amount of $CH_3CH_2O^-$ ions remain constant. Moreover, when the RST is 800 K, a large amount of $CH_3CHO$ molecules are generated, together with a small amount of $CH_2O$ molecules.

For the DEC-$LiPF_6$ electrolyte, $(CH_3CH_2OCO_2)^-$ anions are generated when the RST is 400 K. The amount increases significantly with RST, as can be seen in Fig. 6(b3). When the RST is 700 K, $CH_2O$ molecules are generated in a small amount. In addition, new degradation products emerge, including $CH_3CH_2OH$, $CH_3CH_2OCHO$, and $CH_3CH_2OCOOH$ ($CH_3CH_2OCHO_2$). The number of these molecules generally increase with RST, except the decomposition of $CH_3CH_2OCHO$ and $CH_3CH_2OCOOH$ molecules when the RST is 600 K. Fig. 6(b3) shows that DMC molecules can be generated by secondary reactions of the DEC degradation products. For solvent-phase products having fluorine element, the proportion of $PF_5$ molecules is the largest for EMC-$LiPF_6$ and DEC-$LiPF_6$ electrolytes, as can be seen in Fig. 6(c2) and (c3). A small amount of $CH_3OCO_2CH_2F$ and $CH_3CH_2OCO_2CH_2CH_2F$ molecules are initially generated but then disappear during the thermal degradation process. This can be attributed to the long length of these molecules, which make them less thermally stable. During thermal degradation, the solid-phase product LiF is generated in EMC-$LiPF_6$ and DEC-$LiPF_6$ electrolytes when the RST is higher than 600 K. By contrast, no LiF is observed in the DMC-$LiPF_6$ electrolyte.

Comparing the solvent-phase product generation characteristics in DMC-$LiPF_6$, EMC-$LiPF_6$ and DEC-$LiPF_6$ electrolytes, we can observe an overall trend that the degradation products tend to have smaller molecules when the RST increases. This is because larger molecules tend to have lower thermal stability, and can easily decompose with increasing temperature.

To understand the effect of salt concentration, we performed degradation simulations with another initial salt concentration of $r(LiPF_6) = 0.14$. Fig. 7 shows the number of degraded solvent and salt molecules under different RSTs. The total number of the degraded molecules increase with RST. For DMC-$LiPF_6$, the solvent degradation rate is relatively low at 0.0125/K when the RST increases from 400 K to 800 K. However, the rate increases rapidly to 0.095/K when the RST increases from 800 K to 1000 K. By contrast, the salt degradation rate is relatively stable in Fig. 7(b), which is approximately 0.0275/K within 600 K–1000 K. For EMC-$LiPF_6$ and DEC-$LiPF_6$ electrolytes, the solvent and salt degradation rates are relatively stable, giving 0.076/K and 0.083/K (RST 400 K–700 K) for EMC-$LiPF_6$ and DEC-$LiPF_6$ electrolytes, respectively. The salt degradation rates are 0.026/K for both EMC-$LiPF_6$ and DEC-$LiPF_6$ within RST 400 K–700 K. At the same RST, DEC-$LiPF_6$ has the largest amount of solvent and salt molecules degraded. With a higher salt concentration, the DMC-$LiPF_6$ electrolyte still has the highest thermal stability against thermal degradation, followed by EMC-$LiPF_6$. The DEC-$LiPF_6$ electrolyte still has the lowest thermal stability.

Comparing to a lower salt concentration, the thermal degradation of electrolyte at a higher initial salt concentration is more severe, as can be seen in Fig. 7(c). This trend of increasing initial salt concentration accelerating the electrolyte thermal degradation is consistent with experimental observations [11]. The degraded solvent molecules shows about 6% point increase at the higher salt concentration.

Fig. 8 shows the type and amount of degradation products with an initial salt concentration of $r(LiPF_6) = 0.14$. Comparing to Fig. 6, we can observe that more gas-phase products are generated at a higher salt concentration. In the DMC-$LiPF_6$ electrolyte, the amount of $CH_3F$ molecules initially increases slowly, and then increases rapidly when the RST increases from 800 K to 1000 K. The amount of $CO_2$ molecules initially decreases slightly, and then increases rapidly with continuing thermal degradation. When the RST is

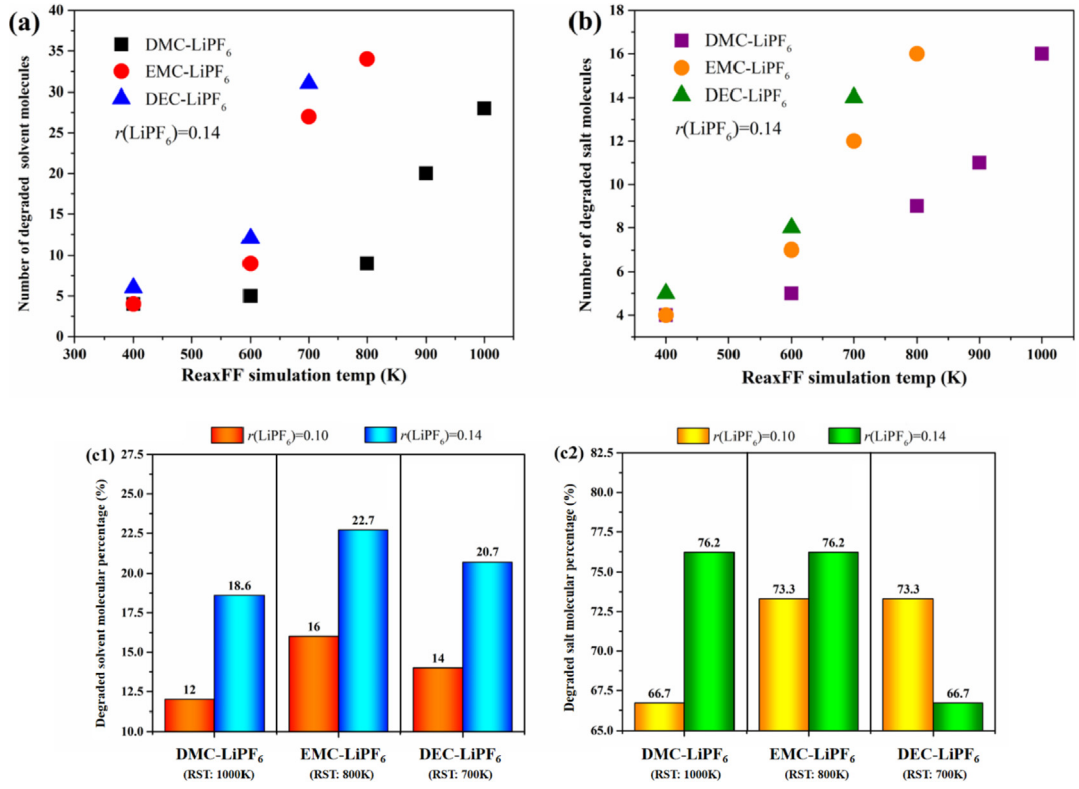


**Fig. 7.** Number of degraded molecules in three electrolytes under various ReaxFF simulation temperatures (RST) (a) solvent molecule, (b) $LiPF_6$ salt molecule, (c) percentage of degraded (c1) solvent molecule and (c2) salt molecule. Salt concentration at $r(LiPF_6) = 0.14$.

1000 K, $CO_2$ molecules are slightly more than $CH_3F$ molecules. A new gas-phase product, $CH_4$, is generated. However, its amount is far less than $CO_2$ and $CH_3F$. For the EMC-$LiPF_6$ electrolyte, $CH_3CH_2F$ molecules emerge when the RST is 400 K. The amount increases with RST. When the RST is 600 K, $CH_3F$, $CO_2$ and $C_2H_4$ molecules are generated. Their amounts increase rapidly with RST. $H_2$ and $CH_4$ molecules are also generated, but their amounts are much smaller. For the DEC-$LiPF_6$ electrolyte, the amount of $CH_3CH_2F$, $C_2H_4$, $H_2$ and $CO_2$ molecules increase with RST. $CH_3CH_2F$ and $C_2H_4$ molecules are much more than $CO_2$ and $H_2$, as can be seen in Fig. 8(a3). When the RST is 700 K, small amount of $C_2H_6$ molecules are generated, which have not been observed at the lower salt concentration in Fig. 6(a3).

Fig. 8(b1) shows the solvent-base products without fluorine element in the DMC-$LiPF_6$ electrolyte. The amount of $CH_3O^-$ anions initially increases slowly and then rapidly with RST. This is the dominating degradation product, similar as Fig. 6(b1). By contrast, the amount of $(CH_3OCO_2)^-$ initially increases but then completely disappears as the RST increases, suggesting that it has a high decomposition rate. A small amount of $CH_2O$ and $CH_3OCHO$ molecules emerge when the RST is 1000 K, which are new solvent-phase products not observed at the lower salt concentration. For the EMC-$LiPF_6$ electrolyte, $(CH3OCO_2)^-$ ions emerges when the RST is 400 K and increase with RST. When the RST is 600 K, $CH_3O^-$ anions, $(CH_3OCO_2)^-$ anions, $CH_3OCOOH$ molecules and $CH_2O$ molecules emerge. The amount of $CH_2O$ increases significantly when the RST increases from 600 K to 800 K, while the amount of $CH_3O^-$, $(CH_3OCO_2)^-$ and $CH_3OCOOH$ increase slightly. Moreover, when the RST is 800 K, similar amount of DMC and $CH_3CH_2OCOOH$ molecules emerge, as can be seen in Fig. 8(b2). For the DEC-$LiPF_6$ electrolyte in Fig. 8(b3), the amount of $(CH_3CH_2OCO_2)^-$ and $CH_3CH_2OH$ increase with RST. $CH_3CH_2O^-$ increases and then decreases with RST. When the RST is 700 K, $CH_3CHO$, $CH_3CH_2OCHO_2$ and $CH_3CH_2OCHO$ molecules are generated. For the solvent-phase products having fluorine element, $PF_5$ is the dominating product among all three types of electrolytes, and it increases with RST. The other products having fluorine element include $CH_3OCO_2CH_2F$, $CH_3CH_2OCO_2CH_2F$, and $CH_3CH_2OCO_2CH_2CH_2F$. These molecules are unstable, and can easily decompose during the thermal degradation process. Their amount is also much smaller than $PF_5$. The solid-phase product is LiF, whose amount is small in comparison to other degradation products.

From the above discussions, it can be seen that for the thermal degradation products of the electrolyte with different initial salt concentrations, the gas phase products of all the three types of electrolytes contain $CO_2$, $H_2$, $CH_4$, $C_2H_4$, $C_2H_6$ and $CH_3CH_2F$. These products have all been confirmed by experiments [3,11,28,29]. The solid phase product of LiF also matches experimental observations, which is a commonly existing product generated by the degradation of $LiPF_6$ [3,11,29]. It should be noted that in an actual LIB, a very small amount of water can be generated by the side reactions from cathode degradation [30]. Water can further react with the electrolyte (especially $LiPF_6$) and generate additional products such as $OPF_3$ [31]. In this research, we focus on the thermal degradation process of the electrolyte itself and therefore ignores the possible existence of trace amount of water.

In order to understand the intrinsic thermal degradation mechanism of electrolytes, we studied the reaction paths. Combining the results for the three types of electrolytes and two salt conditions, we summarize the process in Fig. 9. The detailed reaction formulas are presented in Table 3. We have found 4, 4, and 3 reaction paths for generating the main products in DMC-$LiPF_6$, EMC-$LiPF_6$ and DEC-$LiPF_6$ electrolytes, respectively. The $PF_6^-$ ion tends to decompose first, forming $PF_5$ and ($\cdot$F) ion. The $PF_5$ Lewis acid will promote electrolyte degradation. The C—O bond is easy to decompose with the existence of $PF_5$ molecule [11]. With increasing temperature, more $PF_5$ molecules are generated, as shown in Figs. 5(b) and Fig. 7(b). They cause more solvent molecules to degrade. The detailed process of $PF_5$ molecules attacking the C—O bond is shown in Appendix A.

The DMC molecule can decompose to $(CH_3OCO_2)^-$ anion and $(CH_3)^+$ ion because of C—O bond breaking. As can be seen in Fig. 9(a1), the $(CH_3)^+$ ion reacts with the ($\cdot$F) ion decomposed from $PF_6^-$, forming $CH_3F$. Besides, the DMC molecule can decompose to $CO_2$, $CH_3O^-$ and $(CH_3)^+$ due to C—O bond breaking, especially when the RST is high, as can be seen in Fig. 9(a2) and (a4). Under some

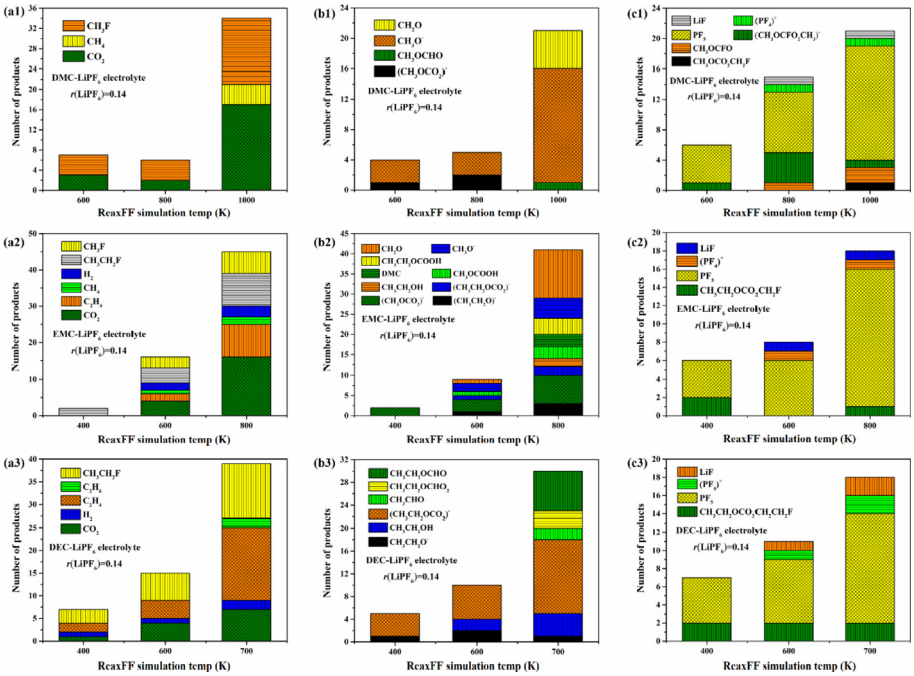


**Fig. 8.** Type and amount of degraded products from ReaxFF MD simulations at a salt concentration of $r(LiPF_6) = 0.14$. (a1-c1) DMC-$LiPF_6$ electrolyte, (a2-c2) EMC-$LiPF_6$ electrolyte, (a3-c3) DEC-$LiPF_6$ electrolyte.

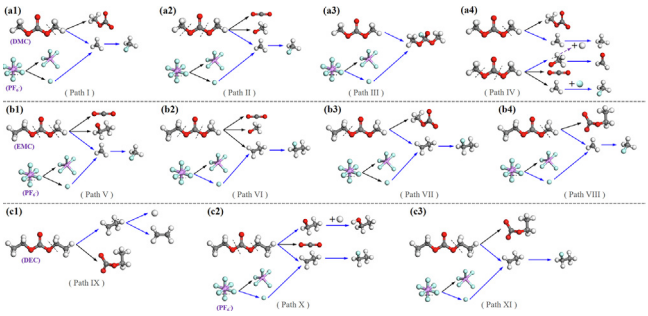

**Fig. 9.** Mechanisms of electrolyte degradation and main product generation by ReaxFF MD simulation at 600 K. (a) DMC-LiPF$_6$ electrolyte, (b) EMC-LiPF$_6$ electrolyte, (c) DEC-LiPF$_6$ electrolyte.

**Table 3**
Thermal degradation reaction of DMC-LiPF$_6$, EMC-LiPF$_6$ and DEC-LiPF$_6$ electrolytes for main product generation based on ReaxFF MD simulations.

| Electrolyte type | Path No. | Process reactions |
|---|---|---|
| _ | – | $PF_6 \rightarrow PF_5 + (\cdot F)$; $Li^+ + (\cdot F) \rightarrow LiF$ |
| DMC-LiPF$_6$ | I | $CH_3OCO_2CH_3 \rightarrow (CH_3OCO_2)^- + (CH_3)^+$;<br>$(CH_3)^+ + (\cdot F) \rightarrow CH_3F$ |
| | II | $CH_3OCO_2CH_3 \rightarrow CO_2 + CH_3O^- + (CH_3)^+$;<br>$(CH_3)^+ + (\cdot F) \rightarrow CH_3F$ |
| | III | $CH_3OCO_2CH_3 + (\cdot F) \rightarrow CH_3OFCO_2CH_3$ |
| | IV | $CH_3OCO_2CH_3 \rightarrow CO_2 + CH_3O^- + (CH_3)^+$;<br>$CH_3OCO_2CH_3 \rightarrow (CH_3OCO_2)^- + (CH_3)^+$;<br>$CH_3O^- \rightarrow CH_2O + (\cdot H)$<br>$(CH_3)^+ + (\cdot H) \rightarrow CH_4$<br>$(CH_3)^+ + (\cdot F) \rightarrow CH_3F$ |
| EMC-LiPF$_6$ | V | $CH_3CH_2OCO_2CH_3 \rightarrow CO_2 + CH_3CH_2O^- + (CH_3)^+$;<br>$(CH_3)^+ + (\cdot F) \rightarrow CH_3F$ |
| | VI | $CH_3CH_2OCO_2CH_3 \rightarrow CO_2 + CH_3O^- + (CH_3CH_2)^+$;<br>$(CH_3CH_2)^+ + (\cdot F) \rightarrow CH_3CH_2F$ |
| | VII | $CH_3CH_2OCO_2CH_3 \rightarrow (CH_3OCO_2)^- + (CH_3CH_2)^+$;<br>$(CH_3CH_2)^+ + (\cdot F) \rightarrow CH_3CH_2F$ |
| | VIII | $CH_3CH_2OCO_2CH_3 \rightarrow (CH_3CH_2OCO_2)^- + (CH_3)^+$;<br>$(CH_3)^+ + (\cdot F) \rightarrow CH_3F$ |
| DEC-LiPF$_6$ | IX | $2CH_3CH_2OCO_2CH_2CH_3 \rightarrow$<br>$2(CH_3CH_2OCO_2)^- + 2(CH_3CH_2)^+$;<br>$2(CH_3CH_2)^+ \rightarrow 2(H)^+ + 2C_2H_4$ |
| | X | $CH_3CH_2OCO_2CH_2CH_3 \rightarrow$<br>$CO_2 + CH_3CH_2O^- + (CH_3CH_2)^+$;<br>$CH_3CH_2O^- + (H)^+ \rightarrow CH_3CH_2OH$<br>$(CH_3CH_2)^+ + (\cdot F) \rightarrow CH_3CH_2F$ |
| | XI | $CH_3CH_2OCO_2CH_2CH_3 \rightarrow (CH_3CH_2OCO_2)^- + (CH_3CH_2)^+$;<br>$(CH_3CH_2)^+ + (\cdot F) \rightarrow CH_3CH_2F$ |

circumstance, the C—H bond inside the $CH_3O^-$ ion can be broken, forming $CH_2O$ molecule and $(\cdot H)$ ion. The $(\cdot H)$ ion can react with $(CH_3)^+$ ion, forming $CH_4$ as shown in Fig. 9(a4). Moreover, the $(\cdot F)$ ion can also react with the DMC molecule directly. The $(\cdot F)$ ion can adhere to the carbon atom in the middle of the DMC molecule, forming $(CH_3OFCO_2CH_3)^-$ anion, as can be seen in Fig. 9(a3).

For the EMC molecule, the C—O bond can also be broken easily. Part of the product has a larger structure than the product of DMC-LiPF$_6$ electrolyte, such as the $CH_3CH_2O^-$ anion, $(CH_3CH_2OCO_2)^-$ anion and $(CH_3CH_2)^+$ ion. The EMC molecule decomposes from C—O bond breaking and forms $CO_2$, $CH_3CH_2O^-$ (or $CH_3O^-$) anion and $(CH_3)^+$ (or $(CH_3CH_2)^+$) ion. As can be seen in Fig. 9(b1) and (b2), the $(CH_3)^+$ or $(CH_3CH_2)^+$ ion reacts with the $(\cdot F)$ ion decomposed from $PF_6^-$, forming $CH_3F$ or $CH_3CH_2F$. In addition, the EMC molecule can also decompose to $(CH_3OCO_2)^-$ anion (or $(CH_3CH_2OCO_2)^-$ anion) and $(CH_3CH_2)^+$ ion (or $(CH_3)^+$ ion), especially when the RST is relatively low, as can be seen in Fig. 9(b3) and (b4).

For the DEC molecule, small solvent-phase molecules and ions, such as $CH_3O^-$ anion, $(CH_3OCO_2)^-$ anion, $(CH_3)^+$ ion etc., do not emerge during the thermal degradation process within RST 400 K—700 K. Although DEC molecule has less thermal stability than DMC and EMC molecules, the degraded products, especially the intermediate products, has a larger molecular structure than that within the DMC-LiPF$_6$, EMC-LiPF$_6$ electrolyte, as can be seen in Fig. 9(c). This phenomenon occurs because two groups of $-CH_3CH_2$ exist in a DEC molecule, while there is only one $-CH_3CH_2$ group in the EMC molecule and no such group in the DMC molecule. The existence of the $-CH_3CH_2$ group provides a higher electron density on the oxygen than the $-CH_3$ group, thus making the DEC molecule to have less thermal stability than the EMC molecule, and making the EMC molecule to have less thermal stability than the DMC molecule [11,32—36]. Besides, the C—H bond in the intermediate products, such as $(CH_3CH_2)^+$ ion, can also be broken. Then the $(H)^+$ ion can be formed, which can react with itself to form $H_2$, or react with $CH_3CH_2O^-$ to form $CH_3CH_2OH$. The $(CH_3CH_2)^+$ ion after C—H bond breaking can form $C_2H_4$, as can be seen in Fig. 9(c1) and (c2).

### 3.3. Results of ionic diffusivity inside degraded electrolyte

After the analysis of the electrolyte thermal degradation process, classical MD simulations were subsequently performed to calculate the ionic diffusivity in the electrolyte after different degrees of thermal degradation. As introduced in section 3.2, the degraded electrolyte products can be divided into three categories, which are gas-phase products (mainly includes $CO_2$, $H_2$, $CH_4$, $C_2H_4$, $C_2H_6$, $CH_3F$ and $CH_3CH_2F$), solvent-phase products (mainly includes $R\text{-}O^-$, $(R—OCO_2)^-$, R—OCHO, R—OCOOH, $CH_3CH_2OH$, $PF_5$, $R—OCO_2CH_2F$, $R—OCO_2CH_2CH_2F$ etc., where R denotes the group of $-CH_3$ or $-CH_3CH_2$), and the solid-phase product (which is LiF). Since the gas-phase and solid-phase degradation products precipitate out of the electrolyte, we include the undegraded solvent molecules, $Li^+$, $PF_6^-$, and solvent-phase products in the simulation system. The number of these particles are calculated based on Figs. 5—8.

Fig. 10 shows the MSD of cations and anions at 333 K. The degree of electrolyte thermal degradation is quantified by the percentage of degraded salt molecules, which is calculated by the ratio between the number of degraded salt molecules and the number of initial salt molecules.

The MSD curves increase linearly with time. The slope of the curves is lower when the electrolyte is more degraded, suggesting slower diffusion. In order to understand the phenomena in detail, we analyzed the solvent structure of the electrolytes after degradation. The solvent structure in this research is represented by the pair correlation between selected particles inside the solvent, which is quantified by the radial distribution function (RDF). RDF can be calculated by

$$g_{a-b}(r) = \frac{n(r)}{4\pi r^2 \delta \rho} \tag{3}$$

where $a$ and $b$ denote different types of particles, $r$ is the radial distance to the center of reference particle $a$, and $n(r)$ denotes the number of $b$ particles whose centers are within the spherical shell of distance $r$ and $r+\delta$ to the center of reference particle $a$, where $\delta$ is the shell thickness. $4\pi r^2\delta$ denotes the volume of the spherical shell, and $\rho$ denotes the number density of $b$ particle, which is calculated by the number of $b$ particles over the simulation cell volume. RDF is a powerful tool in quantifying the pair correlation of selected particles, which can help understand the molecular configurations in electrolytes [12].

The pair correlations of $Li^+$-Oc and $Li^+$-Od, noted as $g_{\text{Li-Oc}}(r)$ and $g_{\text{Li-Od}}(r)$, are investigated first. Here Oc denotes the electronegative carbonyl oxygen in the solvent molecules, while Od denotes the

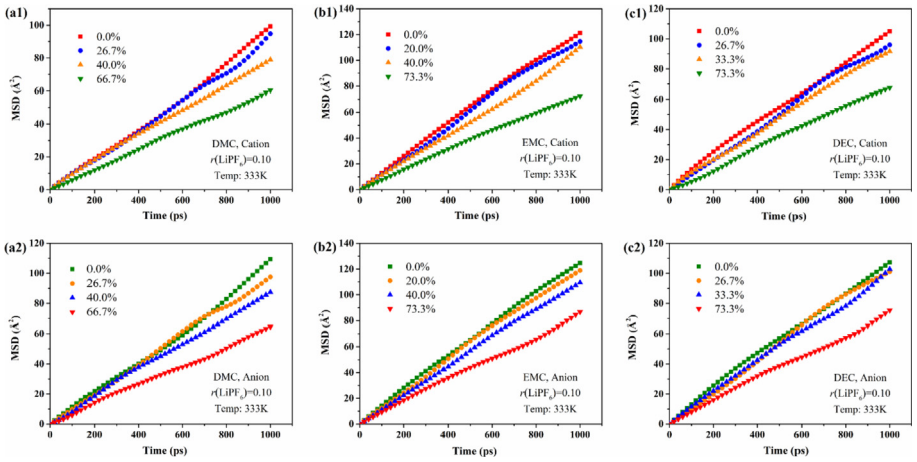


**Fig. 10.** Average MSD of cations and anions in three types of electrolytes with different degrees of degradation ($r(LiPF_6) = 0.10$, Simulation temperature: 333 K) (a) DMC-$LiPF_6$ electrolyte, (b) EMC-$LiPF_6$ electrolyte, (c) DEC-$LiPF_6$ electrolyte.

electronegative oxygen (including electronegative carbonyl oxygen, Oc) in the degradation product molecules. The pair correlation $g_{Li\text{-}Oc}$ $(r)$ can quantify the molecular configuration between $Li^+$ and undegraded solvent molecules, while the pair correlation can quantify the molecular configuration between $Li^+$ and the main products (R-$O^-$ and $(R{-}OCO_2)^-$ anions) degraded from the solvent molecules. Fig. 11 shows the curves of $g_{Li\text{-}Oc}$ $(r)$ and $g_{Li\text{-}Od}$ $(r)$. The positions of Oc and Od are presented in Fig. 11(d1) and (d2).

The RDF curve is relatively smooth for the pair correlation of $Li^+$-Oc, which shows two peaks. The first peak occurs at the same position (2.48 Å from $Li^+$) for different types of electrolytes and at different degrees of degradation. However, the magnitude of the first peak decreases with increasing degree of degradation. The position of the second peak is affected by the degree of degradation as well, as shown in Fig. 11(a1-c1). The position decreases with more degradation. The magnitude of the second peak also decreases slightly with increasing degradation. The RDF curve shows rich features for the pair correlation of $Li^+$ - Od. Multiple peaks can be identified, as shown in Fig. 11(a2-c2). The degraded products of R-$O^-$ and $(R{-}OCO_2)^-$ anions have smaller molecular size than the undegraded solvent molecules. Therefore, these anions are able to surround $Li^+$ ions more closely in a layer-by-layer fashion. The position of the first peak is almost the same for different electrolytes and degrees of degradation (2.41 Å from $Li^+$). The first peak magnitude of $g_{Li\text{-}Od}$ $(r)$ is significantly larger than that of $g_{Li\text{-}Oc}$ $(r)$. The $g_{Li\text{-}Od}$ $(r)$ peaks almost all increase with the degree of degradation. These indicate that $Li^+$ ions can easily adhere to the degradation products of R-$O^-$ and $(R{-}OCO_2)^-$ anions to form clusters of complicated shapes, making it difficult for $Li^+$ ions to adhere to undegraded solvent molecules. The electronegativity of Od atoms in the anions is larger than the Oc atoms in the undegraded solvent molecules, as shown in Fig. 11(d1) and (d2). Therefore, these anions and $Li^+$ ions form dense clusters, which impedes the diffusion of $Li^+$ and anions including R-$O^-$ and $(R{-}OCO_2)^-$. With higher electrolyte degradation, more degradation products of R-$O^-$ and $(R{-}OCO_2)^-$ are generated, as showing in Fig. 6. This makes the cluster larger, which further impedes the diffusion of cations and anions in the degraded electrolyte.

The pair correlation of $Li^+$-$Li^+$ in the three types of electrolytes with different degrees of degradation is also compared and analyzed. Fig. 12 shows the RDF curves of $g_{Li\text{-}Li}$ $(r)$, which are more complicated than the $g_{Li\text{-}Oc}$ $(r)$ curves. When the RDF distance is smaller than 6 Å, the peak magnitude increases with the degree of degradation. However, when the RDF distance is larger than 6 Å, the peak magnitude decreases with the degree of degradation. This indicates that with more degradation, the dense cluster composed of $Li^+$ and anions (including R-$O^-$ and $(R{-}OCO_2)^-$) can absorb more $Li^+$, which can make it more difficult to diffuse in the electrolyte.

Fig. 13 shows the diffusion coefficient of cations and anions in each type of electrolyte, which was calculated based on the MSD curve. The diffusion coefficients all decrease with increasing electrolyte degradation, at an accelerating rate. For each degradation state, the diffusion coefficient increases with temperature. The anions diffuse faster than cations in all electrolytes, and the largest difference occurs in the DMC-$LiPF_6$ electrolyte. Within 0.0%–66.7% electrolyte degradation, the average diffusion coefficient of anions is 9.22%, 24.65% and 34.79% larger than that of cations at 333 K, 303 K and 283 K, respectively in the DMC-$LiPF_6$ electrolyte. Within 0.0%–73.3% electrolyte degradation, the average diffusion coefficient of anions is 6.14%, 7.00% and 9.87% larger than that of the cations in the EMC-$LiPF_6$ electrolyte at the three temperatures. The average diffusion coefficient of anions is 0.61%, 10.57% and 14.46% larger than that of cations in the DEC-$LiPF_6$ electrolyte at the three temperatures.

It can also be seen from Fig. 13 that the diffusion coefficient decreases with degree of degradation. The reduction of ionic diffusivity is relatively slow within 0.0%–30.0% degradation. However, with more than 30.0% degradation, especially when the degree of degradation increases from 40.0% to around 70.0%, the diffusion capability of electrolyte is significantly impacted. This indicates that ion diffusion ability is relatively stable at the beginning of electrolyte thermal degradation, but the ionic diffusivity quickly drops as the electrolyte degradation proceeds.

Fig. 14 shows MSD curves of cations and anions of three types of electrolytes with different degrees of degradation with an initial salt concentration of $r(LiPF_6) = 0.14$. The slope decreases with increasing thermal degradation, suggesting slower diffusion.

The RDF is again used to investigate the solvent structure of the degraded electrolyte. Fig. 15 shows the pair correlation of $Li^+$-Oc and $Li^+$-Od. The position of the first peak is the same as that with $r(LiPF_6) = 0.10$. The magnitude of the $g_{Li\text{-}Oc}$ $(r)$ first peak deceases significantly with increasing degradation in the DMC-$LiPF_6$ and EMC-$LiPF_6$ electrolytes, but only decreases slightly in the DEC-$LiPF_6$ electrolyte. The magnitude of the second peak does not change as much. The magnitude of the $g_{Li\text{-}Od}$ $(r)$ first peak increases with degradation, especially for the DMC-$LiPF_6$ and EMC-$LiPF_6$ electrolytes. The $g_{Li\text{-}Od}$ $(r)$ curve shows more peaks with $r(LiPF_6) = 0.14$ than with $r(LiPF_6) = 0.10$. This is because with a higher initial salt

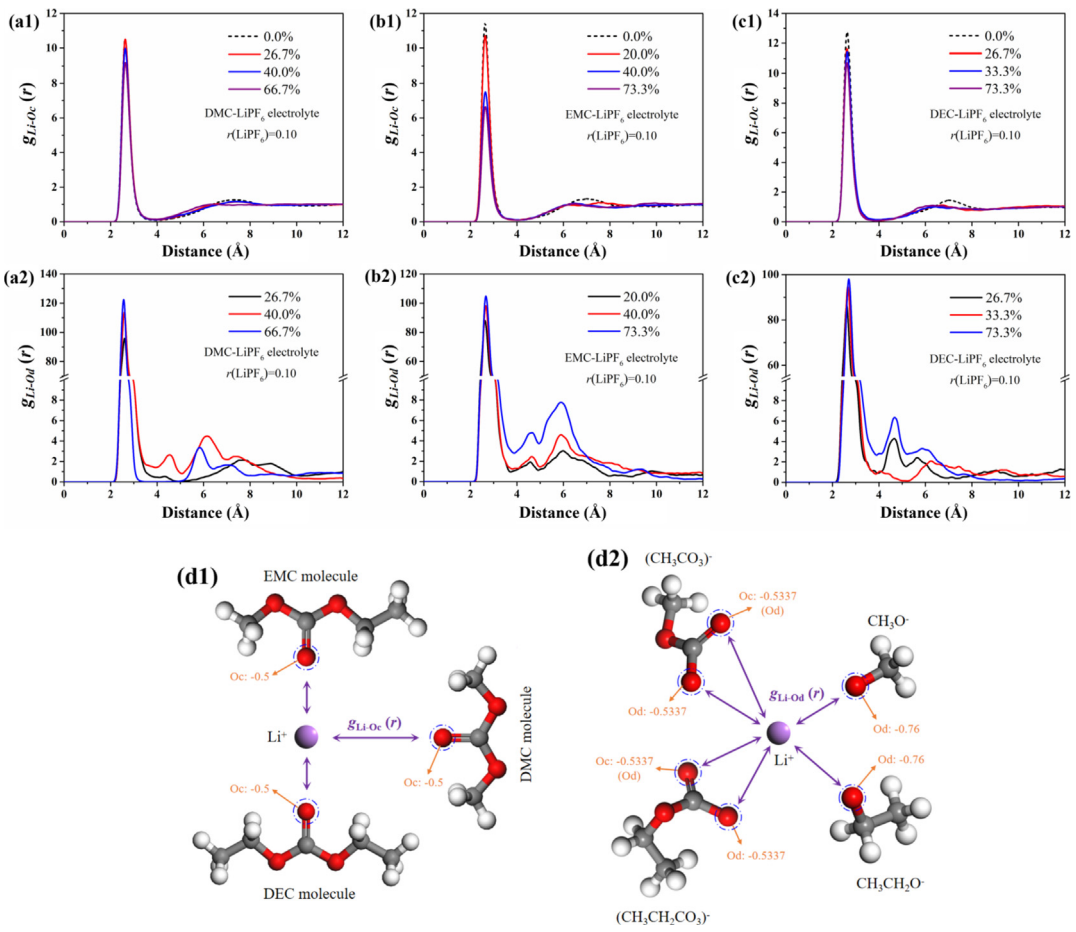


**Fig. 11.** (a1-c1) RDF curves of $Li^+$-Oc ($g_{Li\text{-}Oc}(r)$, Oc denotes the electronegative carbonyl oxygen in the solvent molecules, as presented in Fig. 11(d1)), for three types of electrolytes with different degree of thermal degradation. Simulation temperature: 333 K, $r(LiPF_6) = 0.10$. (a1) DMC-$LiPF_6$ electrolyte, (b1) EMC-$LiPF_6$ electrolyte, (c1) DEC-$LiPF_6$ electrolyte. (a2-c2) RDF curves of $Li^+$-Od ($g_{Li\text{-}Od}(r)$, Od denotes the electronegative oxygen (including electronegative carbonyl oxygen, Oc) in the degradation product molecules, as presented in Fig. 11(d2)), for three types of electrolytes with different degree of thermal degradation. Simulation temperature: 333 K, $r(LiPF_6) = 0.10$. (a2) DMC-$LiPF_6$ electrolyte, (b2) EMC-$LiPF_6$ electrolyte, (c2) DEC-$LiPF_6$ electrolyte.

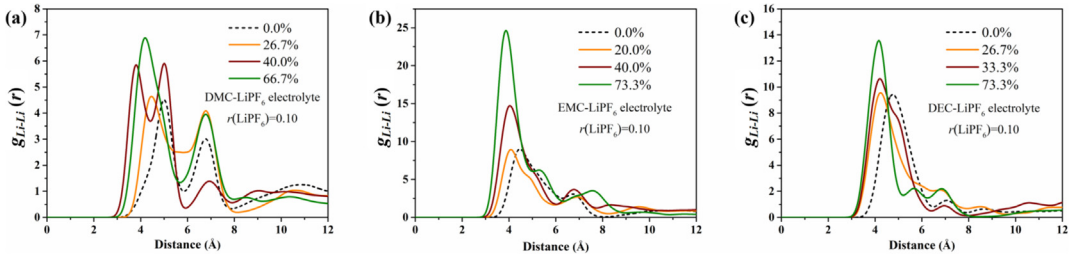


**Fig. 12.** RDF curves of $Li^+$-$Li^+$ ion ($g_{Li\text{-}Li}(r)$) for three types of electrolytes with different degree of thermal degradation. Simulation temperature: 333 K, $r(LiPF_6) = 0.10$. (a) DMC-$LiPF_6$ electrolyte, (b) EMC-$LiPF_6$ electrolyte, (c) DEC-$LiPF_6$ electrolyte.

concentration, more R-$O^-$ and $(R{-}OCO_2)^-$ anions are generated for the same degree of electrolyte degradation, leading to bulk clusters of cations and anions with more complicated structures. Then the RDF curve shows more peaks.

Fig. 16 shows the pair correlation of $Li^+$-$Li^+$. The position of the first peak decreases slightly with degradation, while the magnitude increases significantly as a result of large initial salt concentration. Overall, the RDF curves show similar characteristics between $r(LiPF_6) = 0.14$ and 0.10. $Li^+$ can easily adhere to R-$O^-$ and $(R{-}OCO_2)^-$ anions and form bulk clusters, whose size increases with degradation. These clusters can further absorb more $Li^+$ ions, reducing the diffusion ability of cations and anions in the electrolyte.

Fig. 17 shows the diffusion coefficient of cations and anions. With $r(LiPF_6) = 0.14$, the diffusion coefficient also decreases with electrolyte degradation at an accelerating rate. Anions have higher diffusion coefficients than cations. At 333 K, the largest difference occurs in the EMC-$LiPF_6$ electrolyte. Within 0%–66.5% degradation, the average diffusion coefficient of anions is 10.60%, 6.73% and 6.97% higher than that of the cations in EMC-$LiPF_6$, DMC-$LiPF_6$ and DEC-$LiPF_6$ electrolytes, respectively. However, when the temperature is 303 K and 283 K, the largest difference between anion and cation diffusion occurs in the DMC-$LiPF_6$ electrolyte. Within 0%–

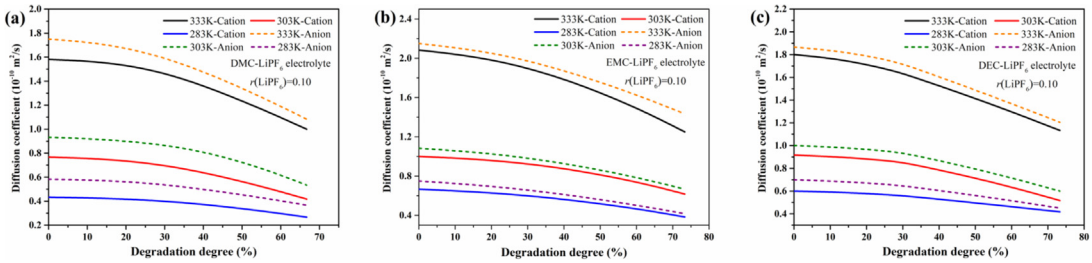


**Fig. 13.** Diffusion coefficient of cations and anions for three types of electrolytes with different degree of thermal degradation. $r(LiPF_6) = 0.10$. (a) DMC-$LiPF_6$ electrolyte, (b) EMC-$LiPF_6$ electrolyte (c) DEC-$LiPF_6$ electrolyte.

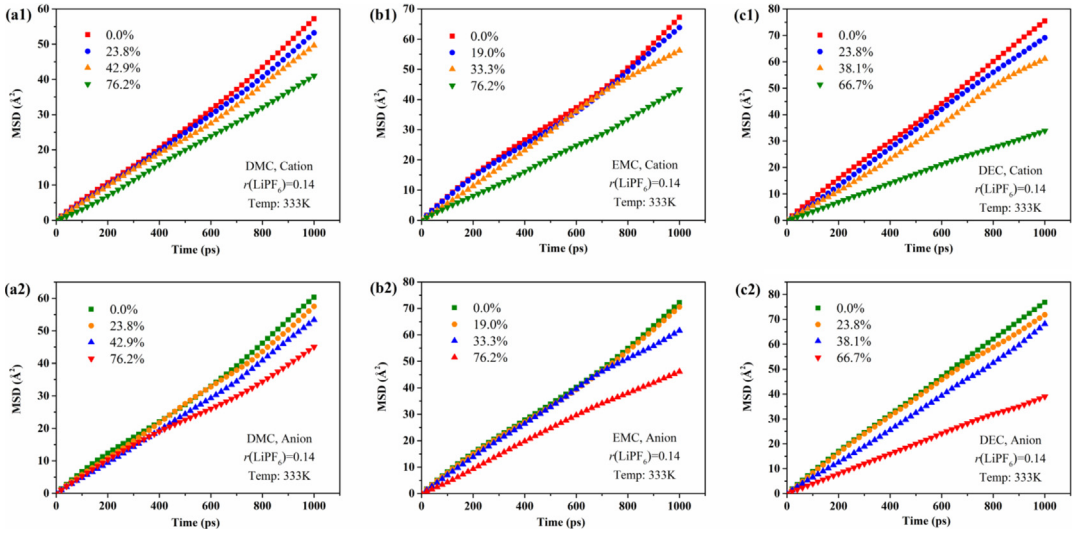


**Fig. 14.** Average MSD of cations and anions in three types of electrolytes with different degree of degradation ($r(LiPF_6) = 0.14$, Simulation temperature: 333 K) (a) DMC-$LiPF_6$ electrolyte, (b) EMC-$LiPF_6$ electrolyte, (c) DEC-$LiPF_6$ electrolyte.

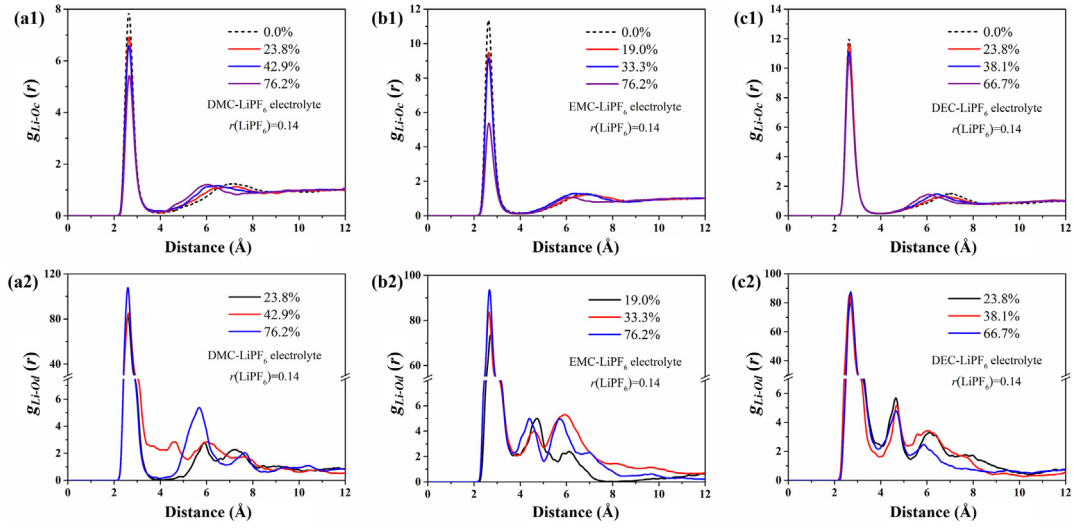


**Fig. 15.** (a1-c1) RDF curves of $Li^+$-Oc for three types of electrolytes with different degree of thermal degradation. Simulation temperature: 333 K, $r(LiPF_6) = 0.14$. (a1) DMC-$LiPF_6$ electrolyte, (b1) EMC-$LiPF_6$ electrolyte, (c1) DEC-$LiPF_6$ electrolyte. (a2-c2) RDF curves of $Li^+$-Od in the degradation product molecules for three types of electrolytes with different degree of thermal degradation. Simulation temperature: 333 K, $r(LiPF_6) = 0.14$. (a2) DMC-$LiPF_6$ electrolyte, (b2) EMC-$LiPF_6$ electrolyte, (c2) DEC-$LiPF_6$ electrolyte.

66.5% degradation, the average diffusion coefficient of anions is 16.68%, 7.75% and 5.90% higher than that of the cations in DMC-$LiPF_6$, EMC-$LiPF_6$ and DEC-$LiPF_6$ electrolytes, respectively at 303 K, and is 41.67%, 4.52% and 24.29% higher than that of the cations in the three electrolytes at 283 K. Fig. 17 also shows that the diffusion coefficient decreases with degradation. Notably, the diffusion coefficient of cations and anions in the DEC-$LiPF_6$ electrolyte decreases slightly between 0% and 25% degradation, but becomes

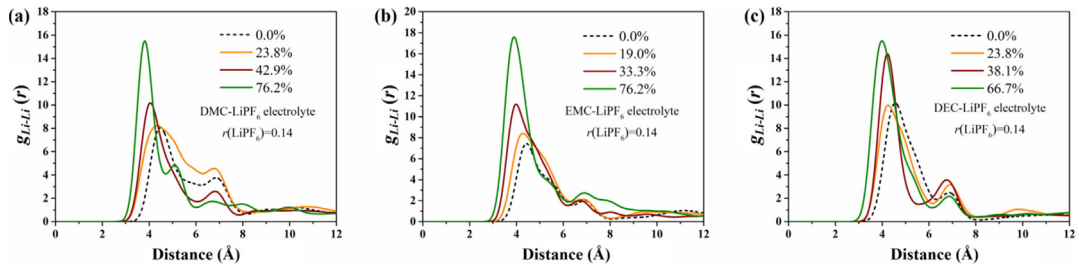


**Fig. 16.** RDF curves of $Li^+$-$Li^+$ ion ($g_{Li\text{-}Li}(r)$) for three types of electrolytes with different degree of thermal degradation. Simulation temperature: 333 K, $r(LiPF_6) = 0.14$. (a) DMC-$LiPF_6$ electrolyte, (b) EMC-$LiPF_6$ electrolyte, (c) DEC-$LiPF_6$ electrolyte.

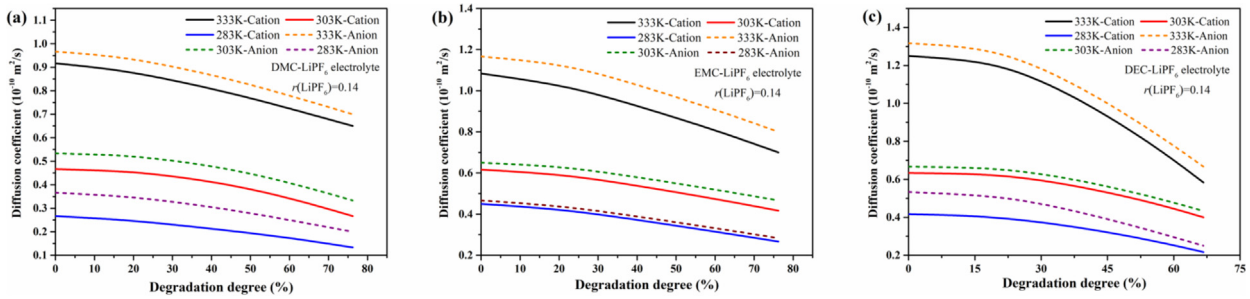


**Fig. 17.** Diffusion coefficient of cations and anions for three types of electrolytes with different degree of thermal degradation. $r(LiPF_6) = 0.14$. (a) DMC-$LiPF_6$ electrolyte, (b) EMC-$LiPF_6$ electrolyte (c) DEC-$LiPF_6$ electrolyte.

much faster from 25% to 65% degradation.

## 4. Conclusions

In this research, the thermal degradation process of major LIB electrolytes and its effect on electrolyte ionic diffusivity were investigated. Three types of electrolytes were chosen for study, including DMC-$LiPF_6$, EMC-$LiPF_6$ and DEC-$LiPF_6$ electrolytes. Classic MD simulations were first used to quantify the diffusivity of electrolytes without thermal degradation under various temperatures and salt concentrations. ReaxFF MD simulations were then employed to provide an atomistic understanding of the thermal degradation process. The ionic diffusivity of degraded electrolytes was further evaluated with classic MD simulations for different temperatures, initial salt concentrations and degrees of thermal degradation. The solvent structures and reaction pathways were identified. Major conclusions are summarized below.

With a salt concentration of $r(LiPF_6) = 0.10$, the EMC-$LiPF_6$ electrolyte has the highest ionic diffusivity, followed by DEC-$LiPF_6$. The DMC-$LiPF_6$ electrolyte has the lowest ionic diffusivity. With a salt concentration of $r(LiPF_6) = 0.14$, the DEC-$LiPF_6$ electrolyte has the highest ionic diffusivity, followed by EMC-$LiPF_6$. This indicates that the ionic diffusivity of DEC-$LiPF_6$ electrolyte is more sensitive to salt concentration. The DMC-$LiPF_6$ electrolyte still has the lowest ionic diffusivity at $r(LiPF_6) = 0.14$. In all cases, the anion has a higher diffusion coefficient than the cation. The results of benchmark MD simulations are consistent with the data from the literature, showing that classical MD simulations are reliable for diffusivity study.

With thermal degradation, the DMC-$LiPF_6$ electrolyte has the highest thermal stability, followed by EMC-$LiPF_6$ and DEC-$LiPF_6$. The $-CH_3CH_2$ group makes the solvent molecules less stable. The degradation of $PF_6^-$ results in $PF_5$, which can further attack the C—O bond in solvent molecules. The thermal degradation products can be classified into gas-phase products including $CO_2$, $H_2$, $CH_4$, $C_2H_4$, $C_2H_6$, R—F (R denotes the group of $-CH_3$ or $-CH_3CH_2$), solvent-phase products with or without fluorine element including R-$O^-$, $(R{-}OCO_2)^-$, R—OCHO, R—OCOOH, $CH_3CH_2OH$, $PF_5$, $R{-}OCO_2CH_2F$, $R{-}OCO_2CH_2CH_2F$ etc., and solid-phase product including LiF. Generally, the thermal degradation products of DMC-$LiPF_6$ electrolyte have smaller molecular structures, while the degradation products of DEC-$LiPF_6$ tend to have larger molecular structures. The large intermediate degradation products tend to decompose further to products of smaller structures.

The diffusion coefficient of cations and anions in the degraded electrolyte decreases with the degree of thermal degradation at an accelerating rate. This effect is closely related to the degradation products of R-$O^-$ and $(R{-}OCO_2)^-$ anions, which attract $Li^+$ cations stronger than the undegraded solvent molecules, forming bulk clusters. As a result, the diffusion of $Li^+$ is reduced. The Od atoms in degraded products have a larger electronegativity than the Oc atoms in undegraded solvent molecules. With increasing degradation, more R-$O^-$ and $(R{-}OCO_2)^-$ anions are generated, promoting the formation of larger bulk clusters that absorb $Li^+$, which cause the decrease of ionic diffusivity.

While this work focuses on the thermal degradation of the electrolyte itself, we would like to note that the ionic diffusion characteristics of electrolyte inside a LIB may also be affected by the electrode during usage. For instance, electrode side reaction and dissolution, electrical field on the electrode surface, and SEI layer can affect the local transport behavior. These are all interesting topics. The approach in this paper may be extended to address these topics in future studies.

## Acknowledgement

The authors gratefully acknowledge the support by the National Science Foundation under Grant No. CNS-1446117 and by LG Chem.

## Appendix A. Detailed simulation for the attacking effect of $PF_5$ molecule on the C—O bond in electrolyte molecules

In order to simulate the effect of $PF_5$ molecule attacking the C—O bond in electrolyte molecules, ReaxFF is employed and the

simulation is conducted with LAMMPS. The DEC molecule is used due to its large $-CH_3CH_2$ group, so that the bond breaking process can be observed more clearly. Three groups of simulations are introduced, where the first group contains 150 DEC molecules, the second group contains 150 DEC and 40 $PF_5$ molecules, and the third group contains 150 DEC and 80 $PF_5$ molecules. The molecular set-ups are shown in Fig. A1.

ReaxFF is employed. The simulation temperature is set to be 600 K for 30 ps in the NVT ensemble with a time step of 0.1 fs. The ReaxFF parameters are the same as those in section 3.

After simulation, the degree of electrolyte degradation and the thermal degradation products are analyzed and shown in Fig. A2. It can be seen from Fig. A2 (a) that when there is no $PF_5$ molecule (group 1), there are only three DEC molecules degraded. When the

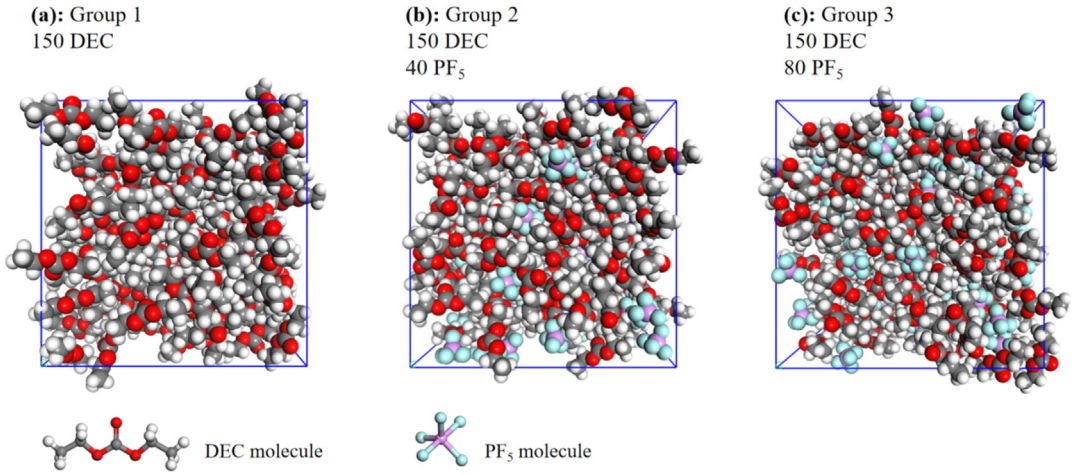


**Fig. A1.** The molecular set-ups of three simulation groups. (a): group 1: 150 DEC molecules. (b) Group 2: 150 DEC and 40 $PF_5$ molecules. (c) Group 3: 150 DEC and 80 $PF_5$ molecules.

For each group, the periodic boundary condition is applied. NPT is firstly employed to relax the system for 500 ps based on the COMPASS force field. The time step is set to be 1 fs. The temperature and pressure are set to be 333 K and 1 atm, respectively. Then the

amount of $PF_5$ molecules in the system increases, the number of degraded DEC molecule increases at an accelerated rate. This trend shows that $PF_5$ can increase the thermal degradation of DEC molecules.

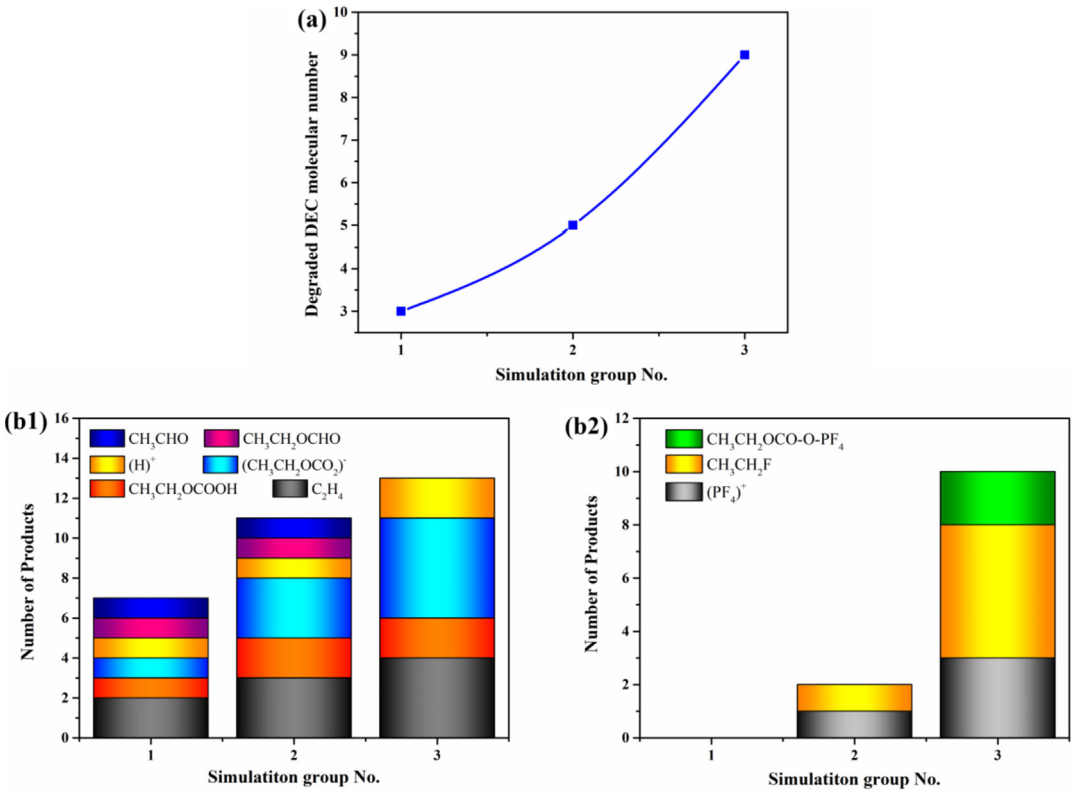


**Fig. A2.** (a): Number of degraded DEC molecules in different groups after simulation. (b1): Electrolyte thermal degradation products without fluorine element. (b2): Electrolyte thermal degradation products with fluorine element.

When there is no $PF_5$ molecule inside the system, the degradation product consists mostly $C_2H_4$ and a smaller amount of $(CH_3CH_2OCO_2)^-$, $CH_3CH_2OCHO$, $CH_3CHO$, $CH_3CH_2OCOOH$ and $(H)^+$, as shown in Fig. A2 (b1). With 40 $PF_5$ molecules (group 2), the product of $C_2H_4$ increases. Notably, the amount of $(CH_3CH_2OCO_2)^-$ ions increases significantly, making it another major product. In addition, a small amount of $PF_5$ molecules degrade, forming $(PF_4)^+$ ions. They react with DEC molecules to form $CH_3CH_2F$ molecules, which can be seen in Fig. A2 (b2). With 80 $PF_5$ molecules, the amount of major products, $C_2H_4$ and $(CH_3CH_2OCO_2)^-$, keeps increasing. The minor products of $CH_3CHO$ and $CH_3CH_2OCOOH$ do not show up in group 3. As for the products containing fluorine element, the amount of $(PF_4)^+$ ions and $CH_3CH_2F$ molecules increases significantly. A new type of product, $CH_3CH_2OC\text{-}O\text{-}PF_4$, emerges in Fig. A2 (b2).

The detailed reaction paths of the DEC solvent during thermal degradation with and without $PF_5$ molecules are shown in Fig. A3 and in Table A1. For group 1 (no $PF_5$), the DEC molecular degradation path can be divided into two paths. In path I, the C—O bond in DEC molecules breaks, forming $(CH_3CH_2)^+$ and $(CH_3CH_2OCO_2)^-$ ions. The $(CH_3CH_2)^+$ ions can further degrade to $(H)^+$ ions and $C_2H_4$ molecules. In path II, the DEC molecules decompose into $(CH_3CH_2OCO)^+$ and $(CH_3CH_2O)^-$ ions from the C—O bond, and combine with $(H)^+$ ion to form $CH_3CH_2OCOOH$ and $CH_3CH_2OH$ molecules. With $PF_5$ molecules added, the C—O bond breaking becomes more significant due to the existence of $PF_5$. The $PF_5$ molecule itself can partly be further decomposed into $(PF_4)^+$ and $(\cdot F)$ ions. These two ions can combine with the DEC molecular degradation intermediate products, and form more stable products such as $CH_3CH_2F$, as path III shows. The $(PF4)^+$ ions can further combine with the $(CH_3CH_2OCO_2)^-$ ions to form $CH_3CH_2OCO\text{-}O\text{-}PF_4$, as shown in path IV. These demonstrate that the existence of $PF_5$ can promote the C—O bond breaking in the DEC molecules. This acceleration effect increases with the amount of $PF_5$ molecules.

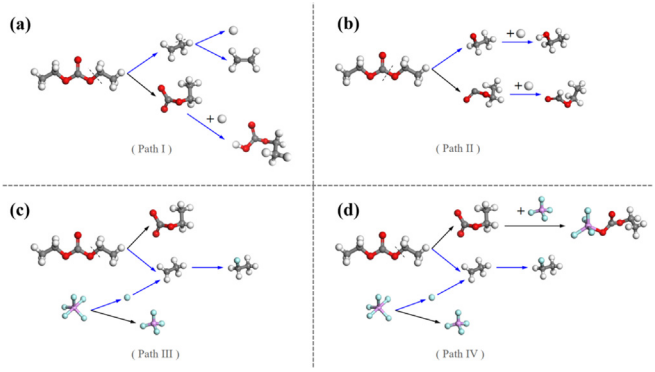


**Fig. A3.** Mechanisms of DEC molecular degradation and main product generation by ReaxFF MD simulation at 600 K. Shown are reaction paths without $PF_5$: (a) Path I, (b) Path II, and reaction paths with $PF_5$: (c) Path III, (d) Path IV.

**Table A1**
Thermal degradation reaction of DEC solvent (I, II without $PF_5$ molecules, and III, IV with $PF_5$ molecules) for main product generation based on ReaxFF MD simulations.

| Path No. | Process reactions | Note |
|---|---|---|
| I | $CH_3CH_2OCO_2CH_2CH_3 \rightarrow$<br>$(CH_3CH_2)^+ + (CH_3CH_2OCO_2)^-$;<br>$(CH_3CH_2)^+ \rightarrow (\cdot H) + C_2H_4$<br>$(CH_3CH_2OCO_2)^- + (\cdot H) \rightarrow CH_3CH_2OCOOH$ | Group 1, Group 2, Group 3 |
| II | $CH_3CH_2OCO_2CH_2CH_3 \rightarrow$<br>$(CH_3CH_2O)^- + (CH_3CH_2OCO)^+$;<br>$(CH_3CH_2O)^- + (H)^+ \rightarrow CH_3CH_2OH$<br>$(CH_3CH_2OCO)^+ + (\cdot H) \rightarrow CH_3CH_2OCHO$ | Group 1, Group 2 |
| III | $CH_3CH_2OCO_2CH_2CH_3 \rightarrow$<br>$(CH_3CH_2)^+ + (CH_3CH_2OCO_2)^-$;<br>$PF_5 \rightarrow (\cdot F) + (PF_4)^+$;<br>$(CH_3CH_2)^+ + (\cdot F) \rightarrow CH_3CH_2F$ | Group 2, Group 3 |
| IV | $CH_3CH_2OCO_2CH_2CH_3 \rightarrow$<br>$(CH_3CH_2)^+ + (CH_3CH_2OCO_2)^-$;<br>$PF_5 \rightarrow (\cdot F) + (PF4)^+$;<br>$(CH_3CH_2)^+ + (\cdot F) \rightarrow CH_3CH_2F$<br>$(CH_3CH_2OCO_2)^- + (PF_4)^+ \rightarrow CH_3CH_2OCO\text{-}O\text{-}PF_4$ | Group 3 |

## References


[1] L. Lu, X. Han, J. Li, J. Hua, M. Ouyang, A review on the key issues for lithium-ion battery management in electric vehicles, J. Power Sources 226 (2013) 272–288, https://doi.org/10.1016/j.jpowsour.2012.10.060.

[2] B. Wu, S. Han, K.G. Shin, W. Lu, Application of artificial neural networks in design of lithium-ion batteries, J. Power Sources 395 (2018) 128–136, https://doi.org/10.1016/j.jpowsour.2018.05.040.

[3] B. Ravdel, K.M. Abraham, R. Gitzendanner, J. DiCarlo, B. Lucht, C. Campion, Thermal stability of lithium-ion battery electrolytes, J. Power Sources 119–121 (2003) 805–810, https://doi.org/10.1016/S0378-7753(03)00257-X.

[4] C.L. Campion, W. Li, B.L. Lucht, Thermal decomposition of LiPF[sub 6]-based electrolytes for lithium-ion batteries, J. Electrochem. Soc. 152 (2005) A2327, https://doi.org/10.1149/1.2083267.

[5] W. Li, C. Campion, B.L. Lucht, B. Ravdel, J. DiCarlo, K.M. Abraham, Additives for stabilizing LiPF[sub 6]-based electrolytes against thermal decomposition, J. Electrochem. Soc. 152 (2005) A1361, https://doi.org/10.1149/1.1926651.

[6] V. Kraft, M. Grützke, W. Weber, J. Menzel, S. Wiemers-Meyer, M. Winter, S. Nowak, Two-dimensional ion chromatography for the separation of ionic organophosphates generated in thermally decomposed lithium hexafluorophosphate-based lithium ion battery electrolytes, J. Chromatogr., A 1409 (2015) 201–209, https://doi.org/10.1016/j.chroma.2015.07.054.

[7] M. Kerner, N. Plylahan, J. Scheers, P. Johansson, Thermal stability and decomposition of lithium bis(fluorosulfonyl)imide (LiFSI) salts, RSC Adv. 6 (2016) 23327–23334, https://doi.org/10.1039/c5ra25048j.

[8] S. Wilken, P. Johansson, P. Jacobsson, Infrared spectroscopy of instantaneous decomposition products of LiPF 6-based lithium battery electrolytes, Solid State Ion. 225 (2012) 608–610, https://doi.org/10.1016/j.ssi.2012.02.004.

[9] P. Handel, G. Fauler, K. Kapper, M. Schmuck, C. Stangl, R. Fischer, F. Uhlig, S. Koller, Thermal aging of electrolytes used in lithium-ion batteries - an investigation of the impact of protic impurities and different housing materials, J. Power Sources 267 (2014) 255–259, https://doi.org/10.1016/j.jpowsour.2014.05.080.

[10] S.F. Lux, I.T. Lucas, E. Pollak, S. Passerini, M. Winter, R. Kostecki, The mechanism of HF formation in LiPF6 based organic carbonate electrolytes, Electrochem. Commun. 14 (2012) 47–50, https://doi.org/10.1016/j.elecom.2011.10.026.

[11] J. Lamb, C.J. Orendorff, E.P. Roth, J. Langendorf, Studies on the thermal breakdown of common Li-ion battery electrolyte components, J. Electrochem. Soc. 162 (2015) A2131–A2135, https://doi.org/10.1149/2.0651510jes.

[12] B. Ravikumar, M. Mynam, B. Rai, Effect of salt concentration on properties of lithium ion battery electrolytes: a molecular dynamics study, J. Phys. Chem. C 122 (2018) 8173–8181, https://doi.org/10.1021/acs.jpcc.8b02072.

[13] N. Kumar, J.M. Seminario, Lithium-ion model behavior in an ethylene carbonate electrolyte using molecular dynamics, J. Phys. Chem. C 120 (2016) 16322–16332, https://doi.org/10.1021/acs.jpcc.6b03709.

[14] M.T. Ong, O. Verners, E.W. Draeger, A.C.T. Van Duin, V. Lordi, J.E. Pask, Lithium ion solvation and diffusion in bulk organic electrolytes from first-principles and classical reactive molecular dynamics, J. Phys. Chem. B 119 (2015) 1535–1545, https://doi.org/10.1021/jp508184f.

[15] A.C.T. Van Duin, S. Dasgupta, F. Lorant, W.A. Goddard, ReaxFF: a reactive force field for hydrocarbons, J. Phys. Chem. A 105 (2001) 9396–9409, https://doi.org/10.1021/jp004368u.

[16] X. Lu, X. Wang, Q. Li, X. Huang, S. Han, G. Wang, A ReaxFF-based molecular dynamics study of the pyrolysis mechanism of polyimide, Polym. Degrad. Stab. 114 (2015) 72–80, https://doi.org/10.1016/j.polymdegradstab.2015.02.004.

[17] Y. Cao, C. Liu, H. Zhang, X. Xu, Q. Li, Thermal decomposition of HFO-1234yf through ReaxFF molecular dynamics simulation, Appl. Therm. Eng. 126 (2017) 330–338, https://doi.org/10.1016/j.applthermaleng.2017.07.104.

[18] K. Chenoweth, S. Cheung, A.C.T. Van Duin, W.A. Goddard, E.M. Kober, Simulations on the thermal decomposition of a poly(dimethylsiloxane) polymer using the ReaxFF reactive force field, J. Am. Chem. Soc. 127 (2005) 7192–7202, https://doi.org/10.1021/ja050980t.

[19] Z. Diao, Y. Zhao, B. Chen, C. Duan, S. Song, ReaxFF reactive force field for

molecular dynamics simulations of epoxy resin thermal decomposition with model compound, J. Anal. Appl. Pyrolysis 104 (2013) 618–624, https://doi.org/10.1016/j.jaap.2013.05.005.
[20] S.S. Han, A.C.T. Van Duin, W.A. Goddard, H.M. Lee, Optimization and application of lithium parameters for the reactive force field, ReaxFF, J. Phys. Chem. A. 109 (2005) 4575–4582, https://doi.org/10.1021/jp051450m.
[21] M. Islam, V.S. Bryantsev, A.C.T. Van Duin, ReaxFF reactive force field simulations on the influence of teflon on electrolyte decomposition during Li/SWCNT anode discharge in lithium-sulfur, Batteries 161 (2014) 3009–3014, https://doi.org/10.1149/2.005408jes.
[22] D. Bedrov, G.D. Smith, Reactions of Singly-Reduced Ethylene Carbonate in Lithium Battery Electrolytes : A Molecular Dynamics Simulation Study Using the ReaxFF, 2012, https://doi.org/10.1021/jp210345b.
[23] R.M. Abolfath, A.C.T. Van Duin, T. Brabec, Reactive Molecular Dynamics Study on the First Steps of DNA Damage by Free Hydroxyl Radicals, 2011, pp. 11045–11049, https://doi.org/10.1021/jp204894m.
[24] J. Liu, X. Guo, ReaxFF molecular dynamics simulation of pyrolysis and combustion of pyridine, Fuel Process. Technol. 161 (2017) 107–115, https://doi.org/10.1016/j.fuproc.2017.03.016.
[25] D. Hong, L. Liu, S. Zhang, X. Guo, Effect of cooling rate on the reaction of volatiles from low-rank coal pyrolysis: molecular dynamics simulations using ReaxFF, Fuel Process. Technol. 178 (2018) 133–138, https://doi.org/10.1016/j.fuproc.2018.05.033.
[26] C.M. Tenney, R.T. Cygan, Analysis of molecular clusters in simulations of lithium-ion battery electrolytes, J. Phys. Chem. C 117 (2013) 24673–24684, https://doi.org/10.1021/jp4039122.
[27] K. Hayamizu, Temperature dependence of self-diffusion coefficients of ions and solvents in ethylene carbonate, propylene carbonate, and diethyl carbonate single solutions and ethylene carbonate + diethyl carbonate binary solutions of LiPF 6 studied by NMR, J. Chem. Eng. Data 57 (2012) 2012–2017, https://doi.org/10.1021/je3003089.
[28] S. Koch, A. Fill, K.P. Birke, Comprehensive gas analysis on large scale automotive lithium-ion cells in thermal runaway, J. Power Sources 398 (2018) 106–112, https://doi.org/10.1016/j.jpowsour.2018.07.051.
[29] E.P. Roth, C.J. Orendorff, How electrolytes influence battery safety, Interf. Mag. 21 (2016) 45–49, https://doi.org/10.1149/2.f04122if.
[30] X. Lin, J. Park, L. Liu, Y. Lee, A.M. Sastry, W. Lu, A comprehensive capacity fade model and analysis for Li-ion batteries, J. Electrochem. Soc. 160 (2013) A1701–A1710, https://doi.org/10.1149/2.040310jes.
[31] B. Gaulupeau, B. Delobel, S. Cahen, S. Fontana, C. Hérold, Real-time mass spectroscopy analysis of Li-ion battery electrolyte degradation under abusive thermal conditions, J. Power Sources 342 (2017) 808–815, https://doi.org/10.1016/j.jpowsour.2016.12.078.
[32] T. Kawamura, S. Okada, J. ichi Yamaki, Decomposition reaction of LiPF6-based electrolytes for lithium ion cells, J. Power Sources 156 (2006) 547–554, https://doi.org/10.1016/j.jpowsour.2005.05.084.
[33] S.E. Sloop, J.K. Pugh, J.B. Kerr, K. Kinoshita, Chemical Reactivity of PF5 and LiPF6 in Ethylene Carbonate/Dimethyl Carbonate, Berkeley Natl. Lab., 2000.
[34] T. Kawamura, A. Kimura, M. Egashira, 2002_Kawamura et al.pdf, 104 (2002) 260–264.
[35] S.E. Sloop, J.B. Kerr, K. Kinoshita, The role of Li-ion battery electrolyte reactivity in performance decline and self-discharge, J. Power Sources 119–121 (2003) 330–337, https://doi.org/10.1016/S0378-7753(03)00149-6.
[36] L. Xing, O. Borodin, G.D. Smith, W. Li, Density functional theory study of the role of anions on the oxidative decomposition reaction of propylene carbonate, J. Phys. Chem. A 115 (2011) 13896–13905, https://doi.org/10.1021/jp206153n.